Transient Postclosure Criticality Model Development

Spent Fuel and Waste Disposition

Prepared for
US Department of Energy
Spent Fuel and Waste Science and Technology

A. Salazar III, C. Sanders, A.A. Alsaed, J. Prouty
Sandia National Laboratories

September 2, 2022

M4SF-22SN010305123
SAND2022-xxxxx X

DISCLAIMER

This information was prepared as an account of work sponsored by an agency of the U.S. Government. Neither the U.S. Government nor any agency thereof, nor any of their employees, makes any warranty, expressed or implied, or assumes any legal liability or responsibility for the accuracy, completeness, or usefulness, of any information, apparatus, product, or process disclosed, or represents that its use would not infringe privately owned rights. References herein to any specific commercial product, process, or service by trade name, trade mark, manufacturer, or otherwise, does not necessarily constitute or imply its endorsement, recommendation, or favoring by the U.S. Government or any agency thereof. The views and opinions of authors expressed herein do not necessarily state or reflect those of the U.S. Government or any agency thereof.

This is a technical report that does not take into account the contractual limitations under the Standard Contract for Disposal of Spent Nuclear Fuel and/or High-Level Radioactive Waste (Standard Contract) (10 CFR Part 961). For example, under the provisions of the Standard Contract, DOE does not consider spent nuclear fuel in multi-assembly canisters to be an acceptable waste form, absent a mutually agreed to contract amendment. To the extent discussions or recommendations in this report conflict with the provisions of the Standard Contract, the Standard Contract governs the obligations of the parties, and this report in no manner supersedes, overrides, or amends the Standard Contract. This report reflects technical work which could support future decision making by DOE. No inferences should be drawn from this paper regarding future actions by DOE, which are limited both by the terms of the Standard Contract and a lack of Congressional appropriations for the Department to fulfill its obligations under the Nuclear Waste Policy Act including licensing and construction of a spent nuclear fuel repository.

Prepared by
Sandia National Laboratories
Albuquerque, New Mexico 87185

U.S. DEPARTMENT OF ENERGY

NNSA National Nuclear Security Administration

Sandia National Laboratories is a multimission laboratory managed and operated by National Technology & Engineering Solutions of Sandia, LLC, a wholly owned subsidiary of Honeywell International Inc., for the U.S. Department of Energy's National Nuclear Security Administration under contract DE-NA0003525. SAND202X-XXXX X.

Sandia National Laboratories

Revision 6
10/7/2019

APPENDIX E
NFCSC DOCUMENT COVER SHEET[1]

Name/Title of Deliverable/Milestone/Revision No.	Transient Postclosure Criticality Model Development
Work Package Title and Number	Probabilistic Post-Closure DPC Criticality Consequence Analyses – SNL SF-22SN01030512
Work Package WBS Number	1.08.01.03.05 Direct Disposal of Dual Purpose Canisters
Responsible Work Package Manager	Laura Price Laura Price (Name/Signature)
Date Submitted	September 2, 2022

Quality Rigor Level for Deliverable/Milestone[2]	☐ QRL-1 ☐ Nuclear Data	☐ QRL-2	☒ QRL-3	☐ QRL-4 Lab QA Program[3]

This deliverable was prepared in accordance with Sandia National Laboratories
(Participant/National Laboratory Name)

QA program which meets the requirements of
☒ DOE Order 414.1 ☐ NQA-1 ☐ Other

This Deliverable was subjected to:

☒ Technical Review ☐ Peer Review

Technical Review (TR) Review Documentation Provided	**Peer Review (PR) Review Documentation Provided**
☐ Signed TR Report or,	☐ Signed PR Report or,
☐ Signed TR Concurrence Sheet or,	☐ Signed PR Concurrence Sheet or,
☒ Signature of TR Reviewer(s) below	☐ Signature of PR Reviewer(s) below

Name and Signature of Reviewers
David Ames

NOTE 1: *Appendix E should be filled out and submitted with the deliverable. Or, if the PICS:NE system permits, completely enter all applicable information in the PICS:NE Deliverable Form. The requirement is to ensure that all applicable information is entered either in the PICS:NE system or by using the NFCSC Document Cover Sheet.*

- *In some cases there may be a milestone where an item is being fabricated, maintenance is being performed on a facility, or a document is being issued through a formal document control process where it specifically calls out a formal review of the document. In these cases, documentation (e.g., inspection report, maintenance request, work planning package documentation or the documented review of the issued document through the document control process) of the completion of the activity, along with the Document Cover Sheet, is sufficient to demonstrate achieving the milestone.*

NOTE 2: *If QRL 1, 2, or 3 is not assigned, then the QRL 4 box must be checked, and the work is understood to be performed using laboratory QA requirements. This includes any deliverable developed in conformance with the respective National Laboratory / Participant, DOE or NNSA-approved QA Program.*

NOTE 3: *If the lab has an NQA-1 program and the work to be conducted requires an NQA-1 program, then the QRL-1 box must be checked in the work Package and on the Appendix E cover sheet and the work must be performed in accordance with the Lab's NQA-1 program. The QRL-4 box should not be checked.*

This page is intentionally left blank.

SUMMARY

A key objective of the United States Department of Energy's (DOE) Office of Nuclear Energy's Spent Fuel and Waste Science and Technology (SFWST) Campaign is to better understand the technical basis, risks, and uncertainty associated with the safe and secure disposition of spent nuclear fuel (SNF) and high-level radioactive waste. Commercial nuclear power generation in the United States has resulted in thousands of metric tons of SNF, the disposal of which is the responsibility of the DOE (Nuclear Waste Policy Act of 1982, as amended). Any repository licensed to dispose of SNF must meet requirements regarding the long-term performance of that repository. For an evaluation of the long-term performance of the repository, one of the events that may need to be considered is the SNF achieving a critical configuration during the postclosure period. Of particular interest is the potential behavior of SNF in dual-purpose canisters (DPCs), which are currently licensed and being used to store and transport SNF but were not designed for permanent geologic disposal.

A multiyear effort was initiated to examine the potential consequences of criticality events with respect to long-term repository performance. These criticality events are postulated to occur during the postclosure period in a hypothetical repository containing DPCs. One of the key challenges is the need to create the modeling tools and techniques that may eventually be required to either exclude criticality from or include criticality in a performance assessment as appropriate. As a result, the effort began with a scoping phase to develop an approach to creating the needed modeling tools and techniques (Price et al. 2019a), followed by a second phase to implement the modeling approach and identify future work (Price et al. 2019b). In subsequent work, the study team considered the relevant features, events, and processes and moved forward with the development of tools and techniques to model the potential consequences of postclosure steady-state criticality as well as transient criticality (Price et al. 2021). The work on modeling steady-state criticality considered multiple canisters in a repository-scale PA while the work on modeling transient criticality focused on a single canister under repository conditions.

This report documents recent advances in the development of transient criticality modeling capabilities. Similar to the steady-state criticality modeling, the transient criticality modeling considers two different geologic reference cases for generic repositories: an unsaturated alluvium repository and a saturated shale repository. Transient criticality modeling focuses on relatively high, reactivity insertion magnitudes (greater than \$1) and the evaluation of the relevant consequences and parameters during the transient, including peak power, total energy release, fuel temperatures, and moderator temperatures.

This work constitutes the second iteration of the transient criticality modeling development effort. A base model for a pressurized water reactor DPC with an example localized reactivity insertion was developed in the first iteration (Price et al. 2021). This second iteration is focused on developing a base model for a pressurized water reactor DPC with an example global reactivity insertion and a boiling water reactor DPC model with localized reactivity insertion. Given that the codes used for modeling transient criticality were developed for engineered power and research reactors, some considerations regarding kinetics and thermal hydraulics were identified warranting improvements to establish modeling parity for repository conditions.

Future iterations of this effort will use the refined base models to address the dependence of the analysis on DPC conditions during a transient (e.g., moderator composition, orientation), potential reactivity insertion conditions (e.g., mechanisms, magnitudes, rates, locations), fuel characteristics (e.g., configuration, burnup, axial and radial profiles), and timing of transient (affects fuel composition and could affect transient kinetics). The current modeling approach assumes that a transient event is initiated in a DPC that is at a steady-state critical condition, with the focus being on evaluation of the initial pulse.

Consideration of a transient event initiating in a DPC from a subcritical state, evaluation of follow-on pulses, and termination into a steady-state critical system are planned for evaluation in future iterations.

At some point, the models developed from this effort will have to be validated. The specific validation techniques will be addressed once workable models are developed and transient credibility is evaluated. Model validation is expected to follow the approach described in Section 3.7.3.1 of the Topical Report (YMP 2003) with any necessary changes based on repository geology and model details.

This report fulfills the SFWST Campaign milestone M4SF-22SN010305123.

ACKNOWLEDGEMENTS

This work was supported by the DOE Office of Nuclear Energy, through the Office of Spent Fuel and Waste Science and Technology.

The authors would like to thank David Ames of Sandia National Laboratories for his technical review, as well as Tim Gunter and Bob Clark from the DOE for their suggestions and guidance.

This page is intentionally left blank

CONTENTS

LIST OF FIGURES

LIST OF TABLES

ACRONYMS

BU	maximum burnup
BWR	boiling water reactor
CFR	Code of Federal Regulations
DOE	US Department of Energy
DPC	dual-purpose canister
EBS	engineered barrier system
ENDF	Evaluated Nuclear Data File
Enr	initial enrichment
FEP	feature, event, and/or process
FE	Federal Register
FTC	fuel temperature coefficient
GE	General Electric
IAPWS	International Association for the Properties of Water and Steam
IF97	Industrial Formulation 1997
MCNP	Monte Carlo N-Particle Transport
MTC	moderator temperature coefficient
MTU	metric tons of uranium
n.d.	no date (an abbreviation used when a reference has no date)
NRC	US Nuclear Regulatory Commission
OTFDB	on-the-fly Doppler broadening
PA	performance assessment
PWR	pressurized water reactor
REA	rod ejection accident
S3K	SIMULATE-3K
SFWST	Spent Fuel and Waste Science Technology
SNF	spent nuclear fuel
TAD	transportation, aging, and disposal
UNF-ST&DARDS	Used Nuclear Fuel – Storage, Transportation & Disposal Analysis Resource and Data Systems
US	United States

This page is intentionally left blank

SPENT FUEL AND WASTE SCIENCE AND TECHNOLOGY

ANALYSIS OF MAGNITUDE AND CONSEQUENCES OF TRANSIENT POSTCLOSURE CRITICALITY

1. INTRODUCTION

One of the objectives of the United States (US) Department of Energy's (DOE) Office of Nuclear Energy's Spent Fuel and Waste Science and Technology (SFWST) Campaign is to better understand the technical basis, risks, and uncertainty associated with the safe and secure disposition of spent nuclear fuel (SNF) and high-level radioactive waste. Commercial nuclear power generation in the US has resulted in thousands of metric tons of SNF, the disposal of which is the responsibility of the DOE (Nuclear Waste Policy Act 1982, as amended [42 U.S.C. 10101 et seq.]). Any repository licensed to dispose the SNF must meet requirements regarding the long-term performance of that repository. For an evaluation of the long-term performance of the repository, one of the events that may need to be considered is the SNF achieving a critical configuration. Of particular interest is the potential behavior of SNF in dual-purpose canisters (DPCs), which are currently being used to store and transport SNF but were not designed for permanent geologic disposal.

A multiyear effort was initiated to examine the potential consequences of criticality events with respect to long-term repository performance. These criticality events are postulated to occur during the postclosure period in a hypothetical repository containing DPCs. One of the key challenges is the need to create the modeling tools and techniques that may eventually be required to either exclude criticality from or include criticality in a performance assessment (PA) as appropriate. As a result, the effort began with a scoping phase to develop an approach to creating the needed modeling tools and techniques (Price et al. 2019a), followed by a second phase to implement the modeling approach and identify future work (Price et al. 2019b). In the subsequent study, the research team considered the relevant features, events, and processes (FEPs) and moved forward with the development of tools and techniques to model the potential consequences of postclosure steady-state criticality as well as transient criticality (Price et al. 2021). The work on modeling steady-state criticality considered multiple canisters in a repository-scale PA while the work on modeling transient criticality focused on a single canister under repository conditions.

This report documents recent advances in the development of transient criticality modeling capabilities. The current work focuses on relatively high reactivity, insertion magnitudes (greater than \$1) and the evaluation of the relevant consequences and parameters during the transient, including peak power, total energy release, fuel temperatures, and moderator temperatures. The remaining subsections of Section 1 provide background information as well as a description of the purpose and scope of this report and the general approach used to model transient criticality. Similar to the steady-state criticality modeling, the transient criticality modeling considers two different geologic reference cases for generic repositories: an unsaturated alluvium repository and a saturated shale repository. Progress made on modeling transient criticality in an unsaturated alluvium repository is presented Section 2 while Section 3 addresses progress made with respect to a saturated shale repository. Section 4 provides a summary along with a discussion of conclusions and recommended future work.

This report fulfills the SFWST Campaign milestone M4SF-22SN010305123.

1.1 Background

The DOE submitted the *Yucca Mountain Repository License Application* (DOE 2008a) to the US Nuclear Regulatory Commission (NRC) in 2008. An update to the license application was completed later in the same year (DOE 2008b) and submitted to the NRC in 2009. The license application included a PA analyzing the long-term performance of the repository consistent with applicable requirements given in the Code of Federal Regulations (CFR): 10 CFR Part 63 and 40 CFR Part 197. In that PA, SNF was assumed to be placed in transportation, aging, and disposal (TAD) canisters specifically designed to transport SNF from its current storage location to Yucca Mountain, store it for aging purposes (if needed), and dispose it in Yucca Mountain. These TAD canisters were designed and planned to be loaded such that the probability of an in-package criticality event during the repository postclosure period was sufficiently low to exclude it from consideration in the PA (DOE 2008b, Section 2.1.2.2). That is, the probability of a criticality event was less than one chance in 10,000 of occurring within 10,000 years after disposal.

However, the license application process was suspended in 2010, TADs were never built, and thus were not available to be loaded with SNF by utilities. Rather, utilities have continued the practice of storing SNF in DPCs designed to meet relevant NRC requirements for the storage and transportation of SNF (10 CFR Part 72 and 10 CFR Part 71, respectively). While DPCs were designed, licensed, and loaded to preclude the possibility of a criticality event during storage and transport of SNF, they were not designed or loaded to preclude the possibility of a criticality event during the regulated postclosure period following disposal, which can be up to 1,000,000 years.

A key requirement for assessing the long-term performance of a repository is that all FEPs must be included in the PA unless the probability of occurrence of the FEP is below a specified limit or the consequences of its occurrence "…(however probable) can be demonstrated not to be significant" (73 Federal Register [FR] 61256). As noted above, for the Yucca Mountain PA, the probability of in-package criticality in TAD canisters during the postclosure period was, by design, less than one chance in 10,000 in 10,000 years after disposal. Thus, postclosure criticality in TAD canisters was excluded from the Yucca Mountain PA based on probability. Based on studies investigating the probability of occurrence of in-package criticality in DPCs during the postclosure performance period, it is not clear that in-package criticality in DPCs can be excluded from a PA based on probability for all geologies (Hardin et al. 2015).

Therefore, if direct disposal of SNF in DPCs in a geologic repository is to be considered, the associated PA for the repository may have to include in-package criticality. The DOE has developed a methodology for addressing the consequences of in-package criticality during the postclosure period (YMP 2003). If the DOE pursues a disposal licensing strategy that excludes in-package criticality in DPCs from the PA based on low consequence rather than low probability, the DOE will have to demonstrate that the consequences of in-package criticality events are not significant in terms of repository performance. Alternatively, if the consequences of in-package criticality events are included in the PA, then the DOE must demonstrate that the regulatory performance standards can still be met. Regardless of the approach, the DOE will need the ability to model the consequences of postclosure in-package criticality events in terms of repository performance.

1.2 Purpose and Scope

This report documents efforts to advance the development of transient criticality modeling tools since the work reported in Price et al. (2021). The purpose of the work described in this report is two-fold: (1) to further understand how a transient criticality might evolve in a DPC that has been disposed of in either an unsaturated alluvial repository or a saturated shale repository, and (2) to build modeling capability that

can be used as these criticality consequence studies progress. The eventual goal is to develop modeling capabilities that can be used to either exclude criticality from a PA based on consequence or can be implemented in a PA if criticality is to be included. The neutronic, kinetic, and thermal-hydraulic processes important to evaluating transient criticality and its potential adverse impacts on repository performance are examined. Output parameters of interest include peak power, total energy, fuel temperature, and water temperature over the course of the simulated transient criticality.

The approach implemented in the criticality consequences study thus far (Price et al. 2019a; 2019b; 2021) and continued herein is consistent with relevant regulations and requirements and uses existing generic models (Mariner et al. 2017; 2018) as much as possible. The approach to modeling transient criticality in particular is discussed further in Section 1.3.

The work discussed in this report focuses solely on the consequences of criticality during the postclosure period, not the probability of occurrence of criticality. The probability of occurrence of postclosure criticality will be researched in the future. The scope is also limited to the consideration of in-package criticality in DPCs only; that is, criticality events external to the waste package, either in the near field or far field, have not been examined. In addition, the only type of waste form considered is commercial SNF in DPCs, and the DPCs are represented by a single DPC using its as-loaded radionuclide inventory and configuration.

1.3 Approach to Modeling Transient Criticality

Criticality events are postulated in DPCs disposed of in generic saturated and unsaturated repositories. There is a wide range of potential criticality events characterized by duration, reactivity insertion rates, reactivity magnitudes, and consequences. The relevant consequences include power, total energy release, fuel composition changes, fuel temperatures, fuel condition, moderator temperature, radiolysis, and pressure; these consequences could impact the source term as the well as the engineered barrier system (EBS) and natural barrier system, and thus, repository performance. Although the spectrum of postulated events is continuous, it was divided in the *Disposal Criticality Analysis Methodology Topical Report* (YMP 2003) into two types of models for the evaluation of credibility and consequences on repository performance, as follows:

- **Steady-State**—The steady-state model applies when the approach to criticality is sufficiently slow to permit the negative feedback mechanisms to hold the k_{eff} close to unity, so that there is no rapid energy release.
- **Transient**—The transient model applies to the case in which the approach to criticality (reactivity insertion) is fairly rapid, causing the k_{eff} to overshoot the value of unity leading to an (initially) exponential increase in power that is coupled to thermal and mechanical effects, until the negative feedback mechanisms cause the k_{eff} to drop back below unity.

Transient criticality, which is the focus of this report, is based upon the premise that a supercritical state is reached through relatively rapid positive reactivity insertions. These reactivity insertions may be introduced by changes in geometric arrangements, reduced parasitic neutron absorption, enhanced neutron moderation (extent or composition), and/or increased neutron reflection. Note that because of the low-enriched nature of commercial SNF in DPCs, fast neutron spectrum criticalities are not credible. Therefore, cases of relevance involve significant levels of water moderation.

Reactivity insertion rates are determined by the specific changes to the system. Changes in geometry due to disruptive events (e.g., seismic events) could occur in a fraction of a second. Sudden changes in geometry due to corrosion and collapse of baskets or dislodging of neutron absorber materials could occur

at a slightly slower rate. Moderator composition changes due to settling of dissolved/suspended neutron absorbers or corrosion products would be on the order of seconds to minutes. Processes slower than seconds or minutes are encompassed in the steady-state criticality model, which is outside the scope of this report. The reactivity insertion mechanisms could result in localized or global reactivity insertions. Localized insertions could occur in one or multiple radial or axial locations within a DPC. Due to the rapid nature of the transient, the primary negative reactivity mechanisms of concern are the fuel temperature coefficient (FTC) and the moderator temperature coefficient (MTC); changes in fuel composition (e.g., depletion/generation of fissile material and fission products) are not expected to contribute significantly to rapid transients due to the minimal burnup and the delay in the generation of key fission products with large absorption cross sections (e.g., ^{135}Xe which is mostly generated from decay of ^{135}I with a half-life of 6.57 hours).

The scope of this effort is limited to relatively high, reactivity insertion magnitudes (greater than $1) and the evaluation of relevant consequences and parameters during the transient, including peak power, total energy release, fuel temperatures, and moderator temperatures. The objective is to develop a transient criticality modeling approach that (1) is representative of the population of pressurized water reactor (PWR) and boiling water reactor (BWR) DPCs, and (2) is either not sensitive to or bounds the variations associated with the following:

- **Specific PWR and BWR Fuel Designs**—There is a wide variety of assembly fuel designs based on lattice, fuel and assembly dimensions, radial and axial enrichment variations, burnable poison loading, blankets, etc.
- **Initial Fuel Enrichment**—There is a wide range of initial enrichments from 2.0 wt% to 5.0 wt% ^{235}U.
- **Assembly Burnup**—The burnup for the current population of SNF assemblies ranges from essentially unburned assemblies to 62 GWd/MTU, which is the current NRC limit (except for some lead test assemblies).
- **Reactor Depletion**—Assemblies are exposed to varying irradiation characteristics based on their location in the core during, generally, three depletion cycles.
- **Decay Time**—A transient criticality event could be postulated essentially anytime after waste package breach and up to millions of years (^{235}U has a half-life of 704 million years)
- **DPC Loading Patterns**—DPCs are loaded based on thermal and radiation considerations, not potential for criticality since criticality is controlled with neutron absorber plates for storage and transportation applications.
- **Axial Profiles**—Axial profiles vary based on reactor irradiation and fuel design.
- **Presence or Absence of Nonfuel Hardware**—Assemblies could be loaded into DPCs with spent burnable poison rods (full or partial), spent control rods (full or partial), or dummy rods.
- **Presence of Damaged Fuel**—There is a wide range of damaged fuel conditions including assemblies with missing fuel rods or fuel in damaged fuel cans. There is also potential for damage to the SNF during disposal.
- **DPC Designs**—DPCs vary in design considerations primarily related to structural, neutron absorber, and heat transfer components, using various materials of construction and geometric arrangements.

- **DPC Capacity**—PWR DPC capacity ranges from 12 to 37 PWR SNF assemblies and BWR DPC capacity ranges from 24 to 89 BWR SNF assemblies.
- **DPC Orientation**—Although the general assumption is that DPCs would be horizontally oriented, geologic processes could result in potential tilting.

A transient criticality event could be associated with various disposal conditions that may impact the neutronic and kinetic characteristics of the system. These conditions include, but are not limited to, the following:

- Fully or partially flooded packages
- Fuel and moderator temperatures at the time of transient initiation, which could affect the FTC and MTC as well as relevant transient parameters (e.g., peak fuel and moderator temperatures)
- Packages potentially subject to pressurization (e.g., small overpack cracks, sealed cracks)
- Moderator composition ranging from pure water to dissolved species from the geologic formation or corroding DPC internals (taking into account the variety of the materials based on the DPC designs)
- Presence of interstitial materials between the assemblies (e.g., intact or partially degraded baskets, partially degraded absorbers). These considerations could be local or global.
- Potential for configurations with positive MTC. This situation could occur in a DPC with significant excess reactivity. A transient initiating in a flooded DPC (that has significant excess reactivity) with nonpure water with a relatively high concentration of neutron absorbers could result in a condition with a positive MTC.

The ultimate utility of the ongoing modeling is to support the evaluation of transient criticality consequences on repository performance. Determination of the probability of a given transient event, which is highly dependent on the repository geology, EBS design, and specific DPC design/loading, is outside the scope of this report. Probability thresholds and event definitions are based on applicable regulation. Level of consequence significance is geology dependent. Sufficient parametric analyses will be performed to eventually support establishing the boundaries for a specific geology (once selected) based on a specific regulation (once developed). These analysis boundaries are illustrated in Figure 1-1.

Given the variety in DPC loading considerations and fuel characteristics (the 12 items in the first list above) and DPC conditions during a transient (the 6 items in the second list above) as well as reactivity insertion mechanisms, rates and magnitudes, the ongoing modeling approach will focus on understanding the impacts of these variations such that a manageable number of representative (or bounding) models are developed. This outcome is achieved by understanding the system response based on changes in a given parameter. Some parameters can be represented/bounded based on current knowledge as informed by relevant criticality accidents, reactor transients, and previous modeling; others require parametric evaluations. The representative/bounding model(s) may not necessarily be the one(s) with the highest peak power because total energy generation might be more significant to EBS performance. Alternatively, a lower total energy transient due to a localized reactivity insertion could be more significant to fuel and cladding condition (including potential for localized cladding oxidation). The fewer the models the more bounding the assumptions would generally have to be. Level of conservatism and granularity in parameter dependence will be determined based on the modeling results and the application for a specific repository geology.

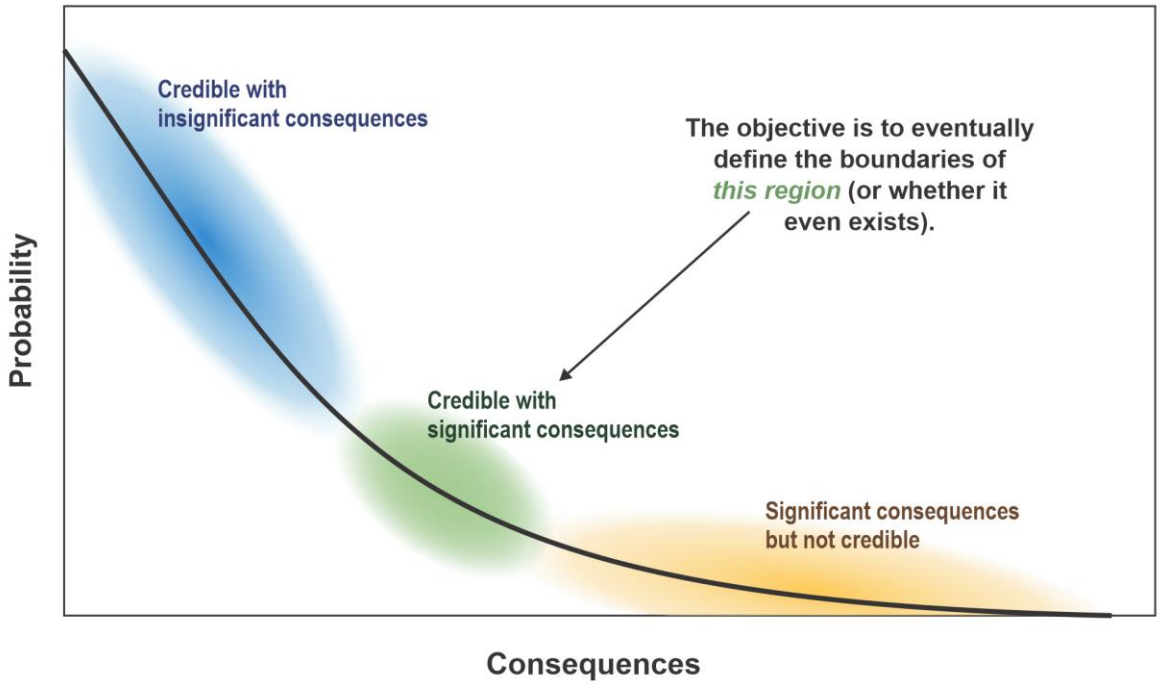

Figure 1-1. Illustration of Criticality Consequence Analysis Boundaries

This report documents the second iteration of this effort. The first iteration (Price et al. 2021) focused on developing a base model for a PWR DPC with an example localized reactivity insertion. This second iteration is focused on developing a base model for a PWR DPC with global reactivity insertion and a BWR DPC model with localized reactivity insertion. Future iterations of this effort will use the base models to address the dependence of the analysis on the parameters discussed above, including DPC conditions during a transient, reactivity insertion mechanisms, fuel characteristics, etc. The current modeling approach assumes that a transient event is initiated in a DPC that is at a steady-state critical condition with focus on the evaluation of the initial pulse. Consideration of a transient event initiating in a DPC from a subcritical state, evaluation of follow-on pulses, or termination into a steady-state critical system will also be evaluated in future iterations.

At some point, the models developed from this effort will have to be validated. The specific validation techniques will be addressed once workable models are developed and transient credibility is evaluated. Model validation is expected to follow the approach described in Section 3.7.3.1 of the Topical Report (YMP 2003) with any necessary changes based on repository geology and model details.

2. MODELING TRANSIENT CRITICALITY IN AN UNSATURATED ALLUVIUM REPOSITORY

2.1 Description of Unsaturated Alluvium Repository

Figure 2-1 depicts the hypothetical reference case for a repository in unsaturated alluvium. The repository depth is 250 m, and waste drifts are backfilled with crushed alluvium (based on Mariner et al. 2018). The drift diameter is 4.5 m, and the maximum percolation rate, corresponding to very wet conditions, is 10 mm/yr. Hydrologic and thermal parameters are given in Table 5-1 of Mariner et al. (2018).

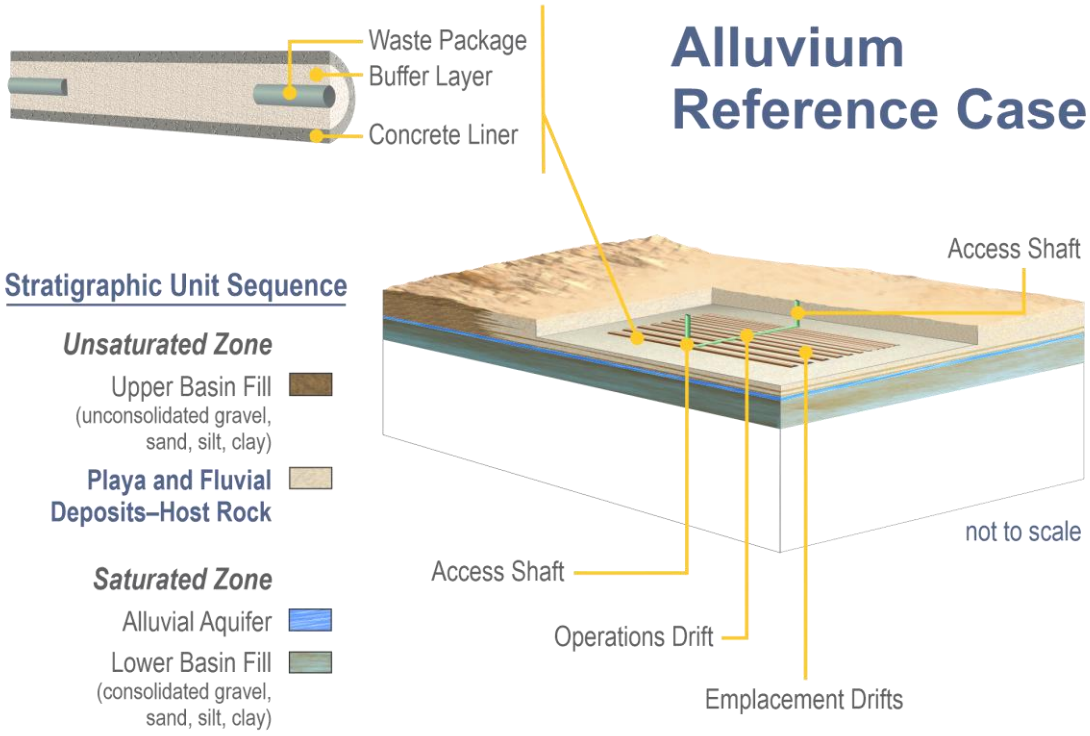

Figure 2-1. Conceptual Drawing of Hypothetical Reference Case for Unsaturated Alluvium

2.2 Objective

This study evaluates the behavior of a potential transient criticality event in a DPC disposed in an unsaturated alluvial repository. The objective is to further the understanding of neutronic, kinetic, and thermal-hydraulic characteristics that could be used in evaluating the extent of potential adverse impacts on repository performance.

Key parameters of interest are the energy release, fuel temperature, and water temperature evolution over the duration of the transient. A reactor kinetics calculation with the RAZORBACK code (Talley 2017a) can illuminate the pulse characteristics given the material properties of the SNF and infiltrated groundwater along with the reactivity insertion characteristics.

For a repository in unsaturated alluvium, the evolution of reactivity as water infiltrates a breached canister and degrades neutron absorbers is investigated as a necessary precursor to the kinetics analysis. A preliminary series of steady-state criticality calculations with the Monte Carlo N-Particle Transport (MCNP) code (Goorley 2014) is conducted to characterize reactivity feedback in a canister with degraded absorbers. Feedback coefficients are then passed to the kinetics analysis to characterize the transient pulse given a positive insertion of reactivity for a given length of time. The time-integrated behavior of the pulse can be used to model effects on the DPC and surrounding barriers in future studies and determine if transient criticality effects are consequential to repository performance.

2.3 Approach

The following subsections describe the approach taken to model a transient criticality event in a DPC disposed in a generic unsaturated alluvial repository.

2.3.1 Model

A DPC is emplaced in a drift in a hypothetical unsaturated alluvium repository and surrounded by crushed alluvium, which is part of an EBS. It is assumed that 20,000 years after disposal, the conditions needed for baseline criticality and a transient criticality event are attained.

An MCNP model has been developed for a 37 PWR DPC with the as-loaded configuration of SNF from the Zion commercial nuclear power station (Price et al. 2021). Unsaturated conditions are modeled with air and various levels of water after the canister is breached, and there is no pressurized, inert, backfill gas remaining. Since the DPC lies at or above the water table, fluid properties are determined at a hydrostatic pressure of 1 atm. While the temperature of the canister is expected to be around 60°C from radioactive decay, the system is modeled at 20.45°C (293.6 K) unless otherwise stated.

The DPC contains 37 Westinghouse 15×15 PWR SNF assemblies with the as-loaded configuration of cask stored at the Zion Nuclear Power Station. The fuel composition was provided by Oak Ridge National Laboratory from depletion calculations on an assembly basis for the cask at Zion using information from Used Nuclear Fuel – Storage, Transportation & Disposal Analysis Resource and Data Systems (UNF-ST&DARDS) (Clarity et al. 2017). The inventory of each assembly is evaluated along 18 axial nodes, and results were postprocessed for direct use in MCNP. Helium and gaseous fission products are assumed to be retained in the UO_2 matrix.

A model of the DPC is shown in Figure 2-2, which depicts assemblies mounted in a basket with 21 square tubes made of carbon steel joined at the corners. These tubes are about 0.8 cm thick and form 16 adjoining void spaces when welded, creating a total of 37 insertion channels with a center-to-center pitch of ~11.8 cm. Outside of the basket, the structural trusses joining the basket to the stainless-steel canister are modeled as empty space filled with fluid.

The inner radius of the canister circumscribes the edges of the basket; an assumed thickness of 1.25 cm results in an outer radius is 91.5 cm. The canister is placed into a 5 cm thick, stainless-steel overpack, which is surrounded by an EBS containing crushed alluvium backfill. However, the neutronics analysis models the area outside of the overpack as vacuum.

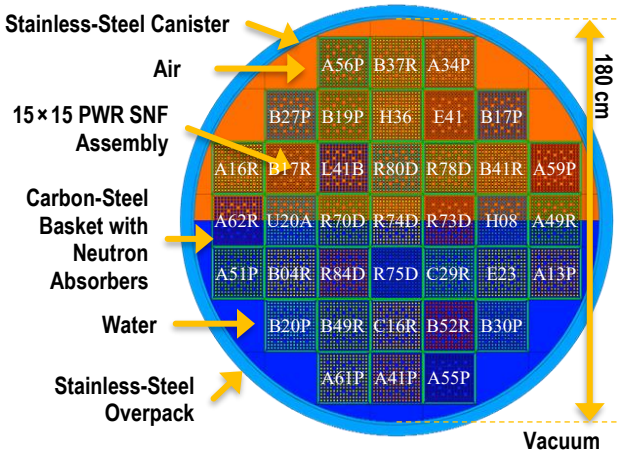

Figure 2-2. Radial Model View of Breached 37 PWR DPC Filled with Air and Water Used for MCNP Calculations

The carbon-steel tubes contain four absorber assemblies of boron carbide (B_4C)/aluminum composite plates mounted internally using stainless-steel retainers. The adjoining void spaces do not contain absorber assemblies. The composite is assumed to contain 65 at% B_4C (43.2 wt%), with boron comprised of the natural abundance of 81.6 wt% ^{11}B and 18.4 wt% ^{10}B. The aluminum component is assumed to be pure ^{27}Al metal with no oxide, and the constituent atoms of the absorber are modeled as a homogeneous mixture.

Fresh fuel dimensions (i.e., prior to reactor operation) are assumed as a conservatism for the neutronics analysis. The fuel rods consist of UO_2 fuel pellets surrounded by a fluid-filled gap and ZIRLO (a zirconium-based alloy) cladding. The fuel has a density (ρ) of 10.2 g/cm^3 (93% of theoretical). The rods and guide tubes are separated by a center-to-center pitch of 1.4 cm, have a uniform length of 400 cm, and include plenum regions outside of the fueled length. Dishing of fuel pellets and gaps between fuel pellets are ignored, making the fuel a continuous cylindrical volume. The SNF is assumed to be disposed with no control rods, allowing for an inspection of the full excess reactivity of the canister. The plenum springs, grid spacers, guide tubes, tie plates, and other nonfuel components (while present physically) are ignored in the neutronics model and replaced with fluid. This assumption results in a high canister void fraction of 75.5% compared to a typical value around 50%.

The axial extent of the DPC is shown in Figure 2-3; centering of the fuel and basket is nonprototypic and employed to reduce the effects of asymmetry. The assemblies are modeled with fluid filling the void spaces above and below them. There are also fluid-filled gaps between the basket and canister lid and between the canister and overpack.

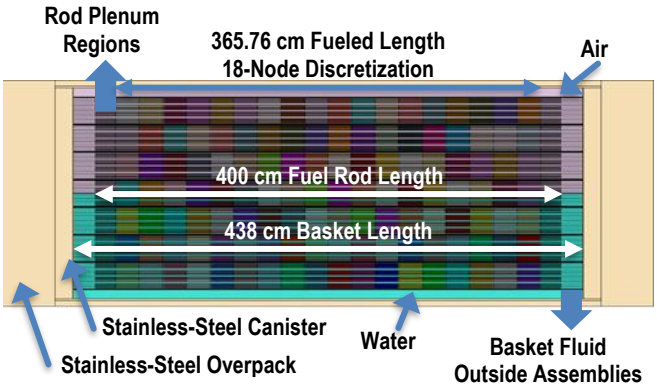

Figure 2-3. Axial Model View of Breached 37 PWR DPC showing Axial Discretization of Assembly Inventories

2.3.2 Neutronics

The MCNP code (version 6.1.1) is used to evaluate effective multiplication (k_{eff}) in the DPC using the canister model and Zion inventories (Goorley 2014). The code and its cross-section libraries have been benchmarked for low-enriched uranium (< 10 wt%) criticality studies via data from the International Criticality Safety Benchmark Evaluation project handbook (Briggs et al. 2003). For criticality calculations, source points defined in each axial fuel node represent neutrons from spontaneous fission or neutrons emitted as a result of decay. Static calculations maintain cross sections from the Evaluated Nuclear Data File (ENDF)/Version B – Rev. 7.1 library at 20.45°C. Calculations incorporating effects of Doppler broadening modify cross sections in the fuel as the temperature increases using the on-the-fly Doppler broadening (OTFDB) code (Martin 2012). Perl scripts are used to incorporate evolving geometries, material compositions and fluid densities into MCNP input files. Thermal scattering models (S[α,β]) are active for water, although the default continuous lwtr.20t library specification at 20.45°C remained fixed if temperature in the water evolved.

2.3.3 Reactivity Insertion Scenario

A DPC is maintained in a subcritical state through the use of neutron absorber plates between the fuel assemblies. In this scenario, after interim storage, the DPC is emplaced in an overpack, which is then emplaced in an alluvial repository and surrounded by crushed alluvium. Upon closure, the overpack is subject to corrosion and other phenomena that can result in a breach and subsequent water infiltration, which could eventually breach the DPC. Extensive degradation of the neutron absorber plates is required to impart the net increases in system reactivity (ρ) needed for criticality. Therefore, the scenario driving the insertion of reactivity into the DPC involves a progressive state of degradation driven by the interaction with groundwater, which is described as follows:

1. The breached canister is initially filled with atmospheric air, and water (conservatively assumed to be pure) infiltrates in incrementally increasing volumes.
2. Per given water level, the wetted portions of the neutron absorber plates are disintegrated, and the boron content of the water is modified.
3. Water infiltrates until the canister is full and all absorber plates have degraded/dissolved homogeneously into solution.

4. The dissolved absorber components precipitate outside of the fuel in the basket, leaving the SNF exposed to fresh water and resulting in a critical state.
5. The water level in the canister is lowered via evaporation due to heat emitted from criticality until a subcritical state is attained once again.

The aluminum-based composite neutron absorber material is expected to degrade within a few hundred years in a repository environment after the canister is breached. The degradation leaves the absorbers susceptible to hydrological transport and displacement from their original locations in the basket. A worst-case scenario would have the absorbers completely transported outside of the assembly slots in the basket. This situation would reduce parasitic absorption and increase interaction between fuel rods in neighboring assemblies, thus increasing reactivity in the DPC.

While the composite absorbers are expected to degrade, they are not expected to dissolve into solution. However, the degradation process is effectively modeled as aqueous dissolution, which is a reasonable approximation since heterogeneous fragments cannot be realistically modeled in MCNP. Therefore, as the water level in the DPC climbs, the B_4C/Al is brought into solution such that the number of molecules is conserved. The portion of the absorber and retainer above the water line is not affected, as shown in Figure 2-4. The stainless-steel retainers have relatively low volume and their effects on neutron transport are assumed to be negligible; therefore, for simplicity, those components are not modeled in solution. Corrosion of the basket, cladding, and grid spacers are ignored to maintain assembly geometry and spacing.

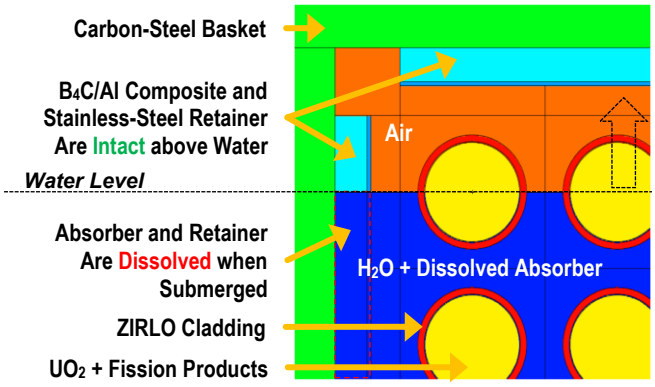

Figure 2-4. Inset of DPC Basket showing Geometry Convention Used for the Degraded Absorber and Retainer

After the B_4C/Al is disintegrated, it is assumed that the material will be transported outside the fuel region of the basket, which may occur because of settling or potential tilting from significant erosion of the EBS or seismic activity. Modeling disintegration as dissolution means that boron forms a precipitate and the quantity of poison in the moderator is reduced, which increases reactivity. Therefore, if the original fuel rod and assembly spacings are maintained, the precipitation of all B_4C/Al outside of fuel region in a water-filled canister provides the full excess reactivity.

2.3.4 Reactivity Feedback

Reactivity feedback is analyzed using a series of steady-state neutronics analyses from the dissolution and precipitation of absorber, loss of moderator, increasing temperature in the fuel, thermal expansion in the fuel, and voiding of the moderator.

The increase in fuel temperature reduces system reactivity through Doppler broadening, which describes a smearing effect of resonances with increasing average temperatures. The peaked resonances for absorption are broadened in energy as a consequence of increased vibrational motion in the target nuclei. This phenomenon results in a depression in absorption cross-section peaks and a spread in the range of applicable energies, with the latter effect ultimately leading to a net increase in absorptions.

For calculations incorporating Doppler broadening effects, cross sections are modified with evolving temperature using the OTFDB code. The code uses ENDF data at various temperatures to create an interpolated energy grid based on a temperature range with set intervals. When a collision is scored in MCNP, OTFDB employs the specific cell temperature to alter both the collision kinematics and absorption cross sections based on the Cullen and Weisbin exact Doppler broadening equation (Cullen and Weisbin 1976).

There are 54 unique nuclides across all materials at 20,000 years. A script was written to run the preprocessor code for these nuclides and create interpolations based on a range of temperatures from 300 K (26.85°C) to 2,500 K (2,226.85°C). The 300 K lower bound is used for rounding purposes, as related ENDF-B/VII.1 evaluations in MCNP include those at 293.6 K and 2,500 K. The upper bound temperature is below the melting point of pure UO_2 fuel (around 2,800°C) but lies above the expected melting point of 2,000°C for zirconium-based alloys. It is also noted that potential for cladding degradation could occur at lower temperatures due to cladding oxidation or pellet-clad interactions. Therefore, the final temperatures in the analysis should cover the point at which significant fuel rod degradation is achieved and a transient criticality event would not be sustainable. Eighth-order interpolations are made in 10 K intervals across this temperature range using an energy grid based on 100 K bins.

RAZORBACK employs the temperature feedback coefficient in the form of the power law shown in Equation 2-1. The coefficients $\mathcal{C}_0$ and $\mathcal{C}_1$ are fitted to the results of the static MCNP calculations with OTFDB to provide an approximation of the temperature feedback coefficient in the fuel, where reactivity is in units of dollars ($\rho_\$$).

$$\partial\rho_\$/\partial T = \mathcal{C}_0 + \mathcal{C}_1/\sqrt{T} \qquad \textit{Equation 2-1}$$

The code also employs feedback coefficients for the coolant in terms of increasing temperature ("spectral") and voiding. The coolant temperature coefficient is implemented as dollar reactivity-per-Kelvin while the voiding coefficient is implemented as dollars-per-percent void. In MCNP, the coolant temperature feedback coefficient is obtained by increasing coolant temperature and modifying coolant density up to 100°C at 1 atm. Pure vapor data are considered unimportant for the transient. The voiding coefficient is found by increasing the steam quality at the 1 atm saturation temperature and using the homogenized density. While the characteristics of two-phase flow would be strongly influenced by the canister geometry and the level of steam separation, the analysis treats the mixture as homogeneous throughout the void space. It is also not practical to model heterogeneous two-phase flow (e.g., bubbles) in the simulation.

The fuel rod gap is modeled as being filled with water as representative of the failed state, as fuel clads are assumed to be breached via corrosion. A helium-filled clad gap (representative of an unbreached clad state) would be a conservative model assumption for the feedback study as it more accurately portrays the role of thermal expansion, given that the system is highly thermal neutronically. The water properties in the coolant analysis are obtained from the International Association for the Properties of Water and Steam (IAPWS) Industrial Formulation 1997 (IF97) for the Thermodynamic Properties of Water and Steam (Wagner et al. 2000). The open-source CoolProp thermophysical property database (version 6.4.1) is used to evaluate this specific formulation for water as well as an equation-of-state for helium (Bell et al. 2014).

2.3.5 Reactor Kinetics

RAZORBACK is a reactor transient analysis code designed to determine the response of a pool-type natural circulation research reactor via a coupled numerical solution of the point kinetics equations, the conservation of energy, and the conservation of momentum for coolant and fuel elements (Talley 2017a). It has been validated for transient analyses with data from the Sandia National Laboratories Annular Core Research Reactor (Talley 2017b). In this study, it is used to evaluate the point kinetics equations given the reactivity feedback behavior in the DPC provided by the neutronics analysis, as it is compatible with the hydrostatic pressure in the alluvium repository (i.e., 1 atm). Calculations are meant to span the applicable time period of the postulated transient pulse for a given total reactivity insertion. In this model framework, a baseline critical state is assumed before the transient, although in-situ events may theoretically proceed from a subcritical state.

In the simulation, the flooded DPC functions as a reactor when absorber plates are degraded (maximum power modeled as 1 MW). The problem employs all 7,548 SNF rods in the DPC and utilizes an element peak-to-average factor of 1.5096 to impart a maximum element power of 0.2 kW for power fraction. Before the transient begins, the problem is allowed to stabilize for 60 seconds with no feedback or reactivity insertion. It then initiates at 100.0% of the full reactor power, with the reactivity insertion beginning at time zero.

The code features reactivity controls in the form of a control rod bank, safety rod bank, and transient rod bank, which impart spatially dependent reactivity effects. There is also an arbitrary time-dependent reactivity addition in the form of a 4^{th}-order polynomial. The calculations presented here use only the time-dependent reactivity addition as means of controlling the reactivity insertion; the addition is ceased after the specified insertion period (i.e., the function is piecewise). The magnitude of the reactivity addition and time period are experimental, while the functional behavior is informed by the neutronics analyses.

Although the DPC is horizontally emplaced, the problem requires the configuration to be vertical to follow the engineered reactor basis of the code and to allow the assemblies to be directly exposed to a column of water acting as a “coolant channel” in a virtual “tank.” The fuel is modeled with length L_{fuel} = 365.76 cm and discretized into 366 nodes (0.999 cm/node). The coolant channel is defined with unheated lengths extending 36 nodes above and below the fueled region to represent both the plenum regions and the void space around the assemblies in the basket. The pool tank height is set as 1,060 cm, providing a maximum 500 cm water column above the coolant channel and 536 cm above the top of the fuel. Assuming an ambient pressure of 14.696 psia and initial water column of 0 cm above the coolant channel, the hydrostatic pressure ranges from 14.7 psia to 20.9 psia from the top of the coolant channel to the bottom. Under these conditions, the boiling point ranges from 100°C to 110°C. The coolant node inlet/exit flow area is 1.36656 cm^2 with a wetted perimeter of 1.45988 cm.

The tank area of 25,543.1 cm^2 represents the area from inner canister radius. There is no other displaced volume in the water apart from the fuel and coolant channel. The pool heating is determined by the DPC power output and natural convection with no active cooling, and the initial pool temperature is set to 60°C. The ANS 5.1 Decay Heat specification is turned on to account for SNF decay heat prior to the transient.

Heat transfer between the liquid coolant and fuel clad is modeled with a single-phase heat transfer coefficient based on a Nusselt number correlation for natural convection. Upon reaching the boiling point, the single-phase heat flux is superposed with the Jens-Lottes subcooled boiling heat flux and Bergles-Rohsenow incipient boiling heat flux to describe the two-phase system.

The fuel is modeled with three zones: cylindrical UO_2 fuel, a clad gap filled with water, and ZIRLO cladding. The clad gap is a necessary initial condition to explore thermal expansion and radiative heat transfer effects in the kinetics study; however, this assumption is not representative of the state of fuel pellets due to reactor irradiation (i.e., swelling, fracturing, and bonding with cladding). A given axial node in the fuel is divided into a number of radial nodes: 30 equally spaced nodes for the UO_2, 10 for the gap, and 10 for the clad. Pressure inside and outside of the fuel element is set initially at 14.696 psia (101,325 Pa), although the outer pressure is fixed.

Table 2-1 shows material properties of the fuel element components as implemented in the RAZORBACK simulation. The densities of UO_2 and ZIRLO are carried over from the neutronics analysis, while that of water (in the clad gap) is fixed at 1.00 g/cm^3. Thermophysical properties of water in the coolant channel are determined from an equation of state.

The MELCOR database is used to determine temperature-dependent thermal conductivity (κ_T) and specific heat (c_p) for UO_2 and ZIRLO (via Zircaloy) (Humphries et al. 2015). Two different temperature ranges are used to define κ_T and c_p for UO_2, where the melting point of 3,113 K marks a transition point for evaluating constant values for the melt. This behavior is applied as a piecewise equation with a polynomial for the solid region and a constant for the melted one.

Table 2-1. Material Properties for a Fuel Element at 1 atm

Material / Property	UO_2	Water (gap)	Helium (gap)	ZIRLO
ϱ [g/cm^3, 20°C]	10.20	1.00	1.66E-4	7.75
κ_T [W/cm·K]	Humphries et al. 2015	Wagner et al. 2000	Bell et al. 2014	Humphries et al. 2015
c_p [J/g·K]				
Emissivity	0.8	0.95	1.0	0.325
Transmissivity	0.0	1.0	1.0	0.0
α [K^{-1}]	Equation 2-2	0.0[a]	0.0[a]	6.721E-6
Young's Modulus [GPa]	180	1.0E-20[b]	1.0E-20[b]	89.9
Poisson's Ratio	0.303	0.3[b]	0.3[b]	0.35

NOTE: [a] RAZORBACK does not expand fluids

[b] Recommended values for gas in RAZORBACK

For UO_2, the default fuel surface emissivity from MELCOR of 0.8 is used. The linear strain from thermal expansion is found from a temperature-dependent fit (Humphries et al. 2015). The linear strain is evaluated from 273.15 K to 2,500 K and then fitted to a 2nd-order polynomial function of temperature (in Kelvin). The derivative of this fit is then taken as the linear thermal expansion coefficient (α) as shown in Equation 2-2.

$$\alpha(T)[K^{-1}] = 5.333 * 10^{-6} + 5.078 * 10^{-9}\, T \qquad \textit{Equation 2-2}$$

For the remaining UO_2 properties, the Young's modulus and Poisson's ratio are derived as average values of published data (Munro 2002). A transmissivity of 0.0 is used to follow the RAZORBACK convention of applying this value for solids; a value of 1.0 is used for gases, where water is assumed to enter the vapor phase during the transient.

For ZIRLO, the surface emissivity is taken from the MELCOR database for conditions of no oxide layer formation. The thermal conductivity is a piecewise temperature-dependent function that is a monotonically increasing polynomial up to 2,098°C and a constant thereafter. The specific heat has more complex behavior, with c_p rising gradually to 1,098°C before rising drastically to a peak. The peak is followed by a drop to a constant value at 1,248°C. The strain from thermal expansion is obtained from a radial fit of Zircaloy data (OECD Nuclear Energy Agency 2016). The strain is evaluated from 273.15 to 2,500 K and then fitted to a line, with the slope providing the thermal expansion coefficient of 6.721×10^{-6}. The Young's modulus and Poisson ratio are based on ZIRLO (Weck et al. 2015).

The axial fission density profile $F_z(z)$ is a polynomial function in axial height incorporating the fuel rod length. The radial fission density profile for a given fuel element is modeled with an exponential function $F_r(r)$. Since the MCNP simulations did not explore this profile through radial discretization of the pellets, the curve was iteratively modified until the integral was normalized with respect to the fuel pellet radius of 0.465 cm. The result is shown in Equation 2-3, where the fission density peaks at the pellet surface.

$$F_r(r) = 0.019 \cdot e^{2 \cdot r} + 0.96866 \qquad \textit{Equation 2-3}$$

The delayed neutron group decay constants and group fractions are taken from an eight-group formulation (Spriggs et al. 1998). Representative values of the total neutron generation time (Λ) and delayed neutron fraction (β_{eff}) are defined as 2.66E-05 seconds and 5.44E-03, respectively, based on preliminary assessments with MCNP. However, MCNP calculations for reactivity feedback employ β_{eff} evaluations obtained from parallel analyses incorporating delayed neutrons.

The reactivity feedback coefficients from the MCNP studies are applied directly and no scaling factors are applied. However, the local feedback weighting factor for the particular location in the fuel element is determined using the product $F_r(r) \cdot F_z(z)$ assuming an exponent of 2.0. This behavior is assumed since the neutronics study did not employ individual rod fidelity. Following fits associated with this choice of exponent, a weighting factor of 0.894 is employed to scale the total reactivity feedback as an adjustment for the core location peaking factor.

2.4 Results

2.4.1 Reactivity Insertion

The first phase of the reactivity insertion involves the infiltration of groundwater into the DPC and the dissolution of absorbers. The reactivity in terms of the rising water level is shown in Figure 2-5. It is shown that the infiltration of water leads to an increase in reactivity, as water provides a neutron moderator as it displaces air. However, this increase is eventually offset with the dissolution of boron from the absorber plates into the water, with the ^{10}B concentration approaching a value of 0.3 at%.

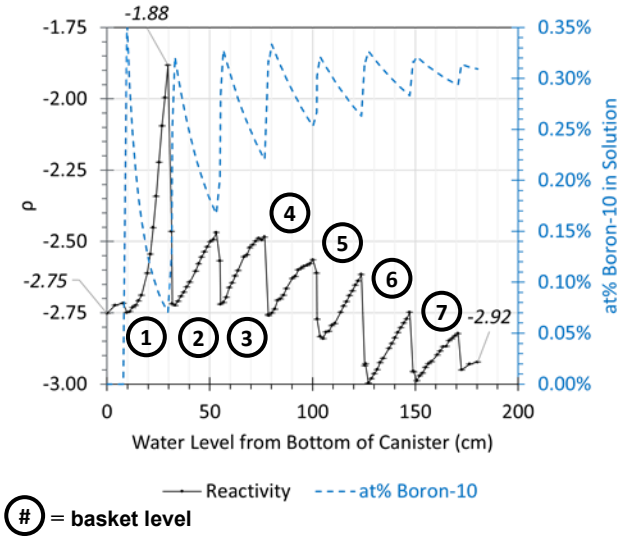

Figure 2-5. Reactivity as Water Infiltrates the Canister and ^{10}B Is Brought into Solution

Ultimately, there is a net decrease in reactivity ($\rho = -2.75 \rightarrow -2.92$, $k_{eff} = 0.26654 \rightarrow 0.25494$) when the canister is full and all the absorber plates have dissolved into solution. This observation shows that dissolving B_4C increases the macroscopic cross section of boron. The reason is the spatial self-shielding effect on the absorber plates, in which thermalized neutrons are preferentially absorbed on the surface of the material while the interior mass is essentially a bystander. If the absorbers remained intact as plates (not in solution), the k_{eff} would be 0.87 at the full water level. It should be noted that this simplifying modeling approach assumes that no precipitation of the dissolved boron occurs until all the absorber plates have degraded.

After the canister fills and the neutron absorber plates dissolve, boron precipitates outside of the fuel regions. As more boron precipitates, the water approaches a pure state and the reactivity in the DPC rises. The reactivity of the DPC as more of the dissolved mass of boron precipitates is shown in Figure 2-6. The system begins with a k_{eff} of 0.25494 and ends with a k_{eff} of 1.04, and criticality ($\rho = 0$) is reached when 99.3% of absorber has precipitated. The system is prompt critical ($\rho_\$ = \$1$) shortly thereafter. The maximum observed reactivity of 0.04 corresponds to a \$6.67 insertion.

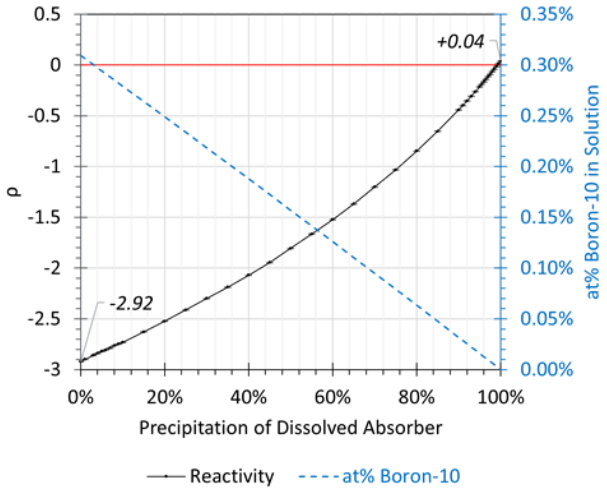

Figure 2-6. Reactivity as the Percentage of Boron in Solution Precipitates outside of the Fuel Region

With no absorbers remaining in the basket, the reactivity of the system drops as the water level decreases from the combined heat of criticality and decay, as shown in Figure 2-7. The reactivity is observed to fall from 0.04 (k_{eff} = 1.04) to −2.43 (k_{eff} = 0.29). Using the bisection method, the baseline critical water level is found as 93.332 cm from the bottom of canister or 3.162 cm above the midplane, which is equivalent to about 2.5 fuel rod pitches. This outcome suggests that with absorber disintegration, the DPC can become critical when 52.2 vol% of the internal void space is flooded. Therefore, these results for the reactivity insertion scenario provide bounds for the occurrence of criticality in unsaturated geology, as the parameter space of poison content and water level has been fully evaluated.

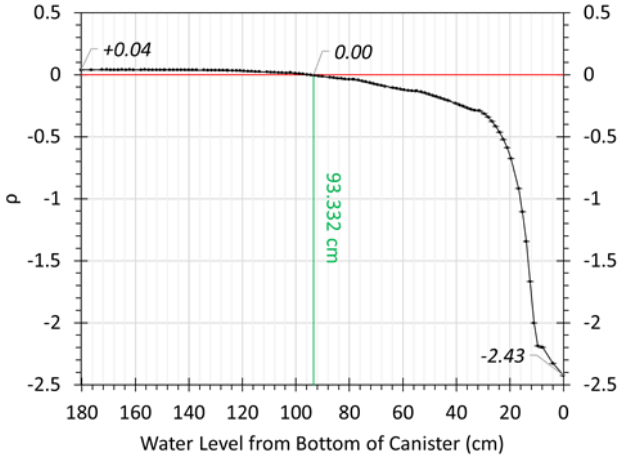

Figure 2-7. Reactivity as the Water Level in the Canister Drops, where Subcriticality Is Reached at 93.3 cm Water Column Height with Respect to the Bottom of the DPC

2.4.2 Fission Power Distribution

The axial fission power distribution $F_z(z)$ was evaluated using the CINDER depletion module in MCNP for the fully inundated canister with no absorber. To represent the conditions of the transient criticality event, time steps were analyzed in logarithmic steps from 1 millisecond to 100 seconds for a power output of 1 MW. Due to memory limitations, only the central assembly in the basket (labeled R74D) was evaluated. The resulting fission power fraction distribution at 100 seconds is shown in Figure 2-8, which shows peaking near one end of the assembly. Since the canister is emplaced horizontally, there is no top or bottom; however, the peak is associated with the top of the active fuel region.

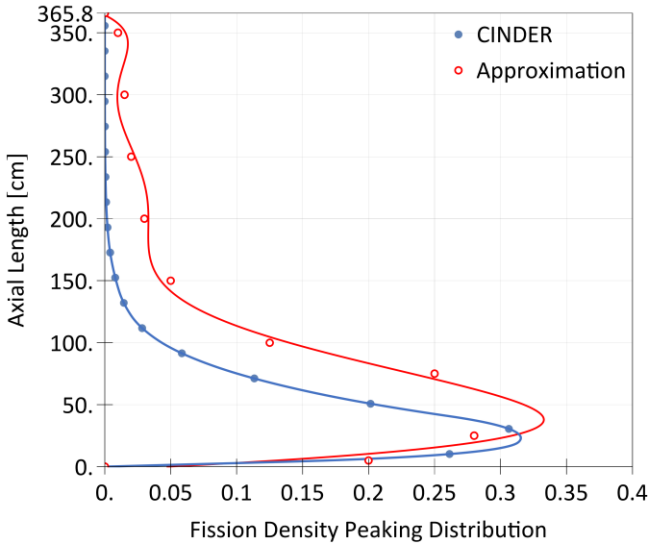

Figure 2-8. Axial Fission Power Fraction Distribution Observed in Assembly R74D at the Center of the Basket along with a 6th-Order Polynomial Approximation based on Nearby Points

RAZORBACK can incorporate custom power distributions using a 6th-order polynomial function, as shown in Equation 2-4. While the polynomial was found to be inaccurate in representing the curve (which conforms to a Gaussian or exponentially modified Gaussian), an approximate fit was found using points in some proximity to the CINDER results (Figure 2-8). This approximation is acceptable considering that the B_4C/Al in water may settle nonuniformly across the DPC and cause depressions in the flux in certain locations. The coefficients of the approximating polynomial are shown in Table 2-2, which are normalized such that the integral of Equation 2-4 from 0 to L_{fuel} is precisely 365.76 cm, as shown in Equation 2-5.

$$F_z(z) =\cdot \sum_{n=0}^{6} a_n \left(\frac{z}{L_{fuel}}\right)^n \qquad \textit{Equation 2-4}$$

Table 2-2. Coefficients Used in Equation 2-4 for the Axial Power Density Distribution

n	a_n
0	0.516
1	73.497
2	−578.847
3	1,777.642
4	−2,668.881
5	1,957.890
6	−561.849

$$\frac{\int_0^{L_{fuel}} F_z(z)}{L_{fuel}} = 1 \qquad \textit{Equation 2-5}$$

Given the incongruence of the system with engineered reactors, the study can iterate on the axial distribution to assess the effects on the final results. Since the DPC is modeled as being vertically emplaced, it is not clear whether the location of the power peak with respect to the water column will significantly affect results. In a horizontal emplacement, the peak location could be on either side of the DPC midplane and be subject to the same hydrostatic pressure.

2.4.3 Reactivity Feedback

The temperature feedback coefficients in the fuel and moderator ("coolant") were estimated in a series of neutronics calculations. For the fuel, this effort involved sequentially broadening the UO_2 cross sections with increasing fuel temperatures while maintaining external materials at 300 K. The temperature range of 300 K–2,500 K was used to apply the OTFDB lookup tables up to cladding failure. The analysis assumed a rapid increase in fuel temperature such that (1) no significant heat is transferred to the surroundings, allowing non-UO_2 components to be fixed with cross sections at 300 K, and (2) the material properties are unaffected with the fuel geometry remaining intact.

The reactivity results are shown in Figure 2-9 and include a $\sqrt{T}$ fit aligning with Equation 2-1. Progressing from 300 K to 2,500 K results in a reactivity drop from \$6.65 to \$1.13, and the critical configuration is maintained up to 2,500 K (2,226.85°C). Therefore, while Doppler broadening alone cannot bring the system to subcriticality, extreme heating of the fuel would result in the melting of cladding and the loss of critical configuration. Using the $\sqrt{T}$ fit to dollars and taking the derivative, the feedback coefficient from Doppler broadening is $-0.082/\sqrt{T}$ \$/K. A generic power-law fit of the results was obtained as $-0.058/T^{0.45}$ \$/K, where the exponent is very close to the $T^{-0.5}$ assumption used in RAZORBACK. The behavior observed in these results contrasts with those to be shown for the distributed Doppler feedback coefficient for the saturated study (Figure 3-7) as a consequence of different analytical approaches, not from differences in geology (i.e., unsaturated versus saturated).

The analysis for the coolant temperature feedback coefficient was conducted by varying the temperature and density of all water infiltrating the canister, including the fuel rod gaps, the tube/void cavities, the space outside of the basket, and the canister/overpack gaps. (Any water trapped in the UO_2 fuel matrix was excluded.) The densities for liquid water at 101,325 Pa are used up to the vapor point, terminating at 373.1243 K (99.9740°C). The results are shown in Figure 2-10, where reactivity is shown to decrease with increasing coolant temperature and decreasing liquid density. The total extent of wetted volumes in the DPC (including gaps) is likely to be an influence of the noticeable error in the plot. Using a linear fit to temperature and taking the derivative, the feedback coefficient was found to be −0.011 $/K.

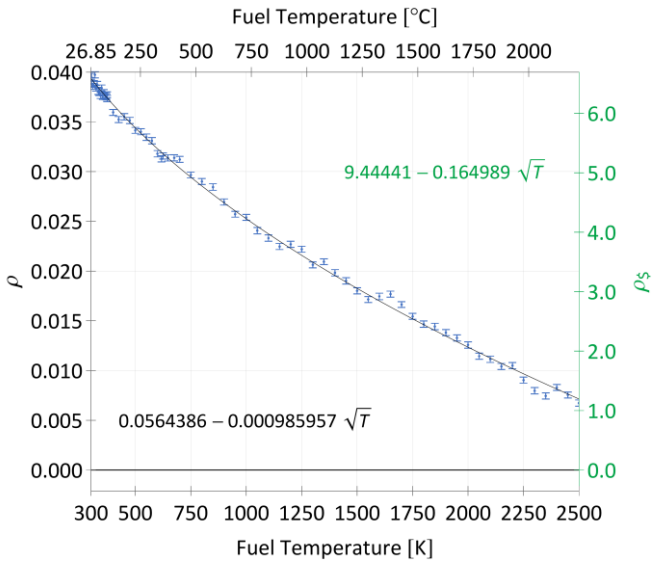

Figure 2-9. Reactivity as the Temperature in the UO_2 Increases

The void coefficient is evaluated for saturated water/steam at 99.9740°C at various steam qualities determined with IF97. The density is modeled as homogenous and a function of quality, and there is no modeling of heterogeneous bubble or steam layers. The results are fit based on the relative change in coolant density compared to the saturated liquid at 1 atm (0.958 g/cm^3). Results are shown in Figure 2-11, where the reactivity decreases from $5.86 with the saturated liquid (0% quality) to $0 at 21.45% density reduction (0.02% quality). A linear fit of the results to dollars yields a feedback coefficient of −0.284 $/%void. It should be noted, however, that the behavior is slightly nonlinear and perhaps could be better described by a different functional form.

The thermal expansion coefficients are obtained by varying the fuel and cladding dimensions. These geometric changes are implemented at fixed temperature (293.6 K) to decouple temperature dependence on the expanding geometry. When the fuel or clad geometry is changed, the densities and volumes listed in the MCNP input deck are also modified while conserving the original mass from the fresh fuel specification. Also, for instances with the fuel and clad in contact, the clad gap region was commented from the fuel rod geometry model. Expansion was acknowledged only in the radial direction with axial lengths kept constant, and in this study, water remains in the clad gap until the gap is closed.

For the fuel, the outer radius of the UO_2 pellet was varied from the engineered specification (0.465 cm) until it pressed directly against the inner wall of the ZIRLO cladding (0.474 cm). The total mass of fuel is

maintained constant, so dimensional changes are met with a change in fuel density. Figure 2-12 shows that, as the fuel expands and becomes less dense, reactivity decreases as the interstitial water between the fuel and cladding is expelled and its moderating effects are reduced, which leads to spectrum hardening. The effects from this interstitial water may also be the cause of significant noise in the results, so a study with void in the gap may be preferable. The thermal expansion feedback coefficients are found from linear fits of the results as −41.757 \$/cm +0.980 \$/(g/cm^3).

Thermal expansion analyses were then performed on the cladding for the inner radius and outer radius (0.536 cm) in separate analyses; reactivity results are shown in Figure 2-13 and Figure 2-14, respectively. While the inner clad was expanded to the point of contact with the fuel, the outer radius was expanded arbitrarily to obtain a satisfactory number of points for fitting, hence the greater spread of results. The feedback coefficient for the clad density change is taken from the outer radius since the magnitude of the coefficient is based on a greater number of points and larger (+0.851 \$/(g/cm^3) compared to +0.281 \$/(g/cm^3)). For radial changes, the feedback coefficient is +28.891 \$/cm for the inner radius is and −60.502 \$/cm for the outer radius. To clarify, in this study, the clad gap is maintained and includes the effect of decreasing quantities of moderator as the gap closes with thermal expansion.

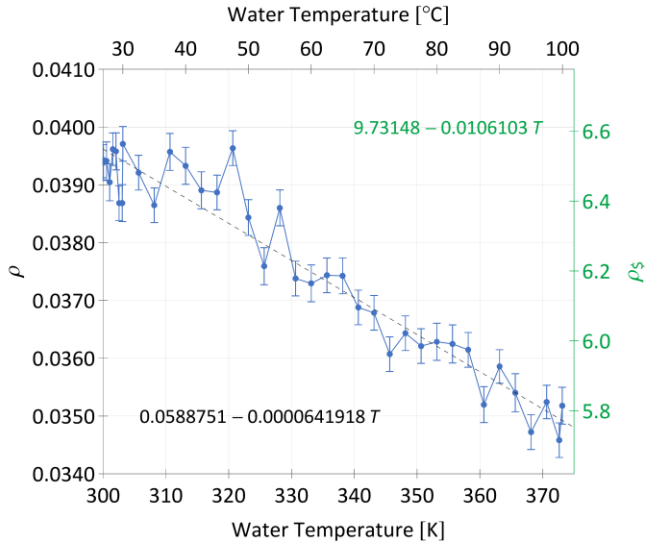

Figure 2-10. Reactivity as the Temperature in the Infiltrated Groundwater Increases and Liquid Density Decreases

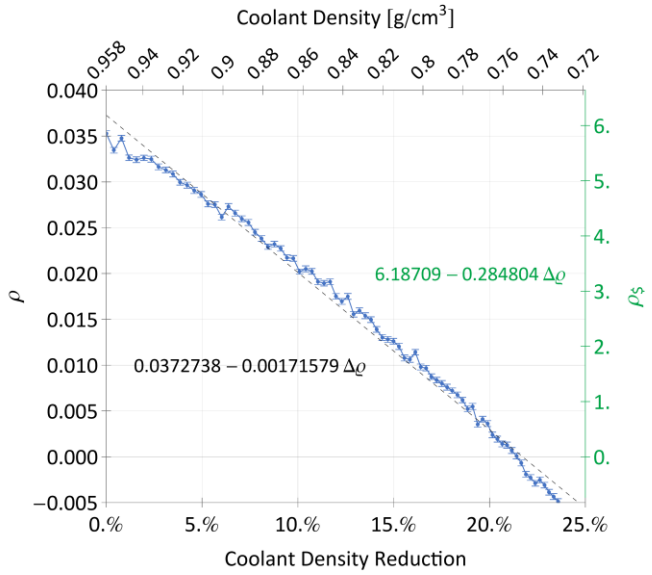

Figure 2-11. Reactivity as the Saturated Coolant Density Is Reduced with Voiding

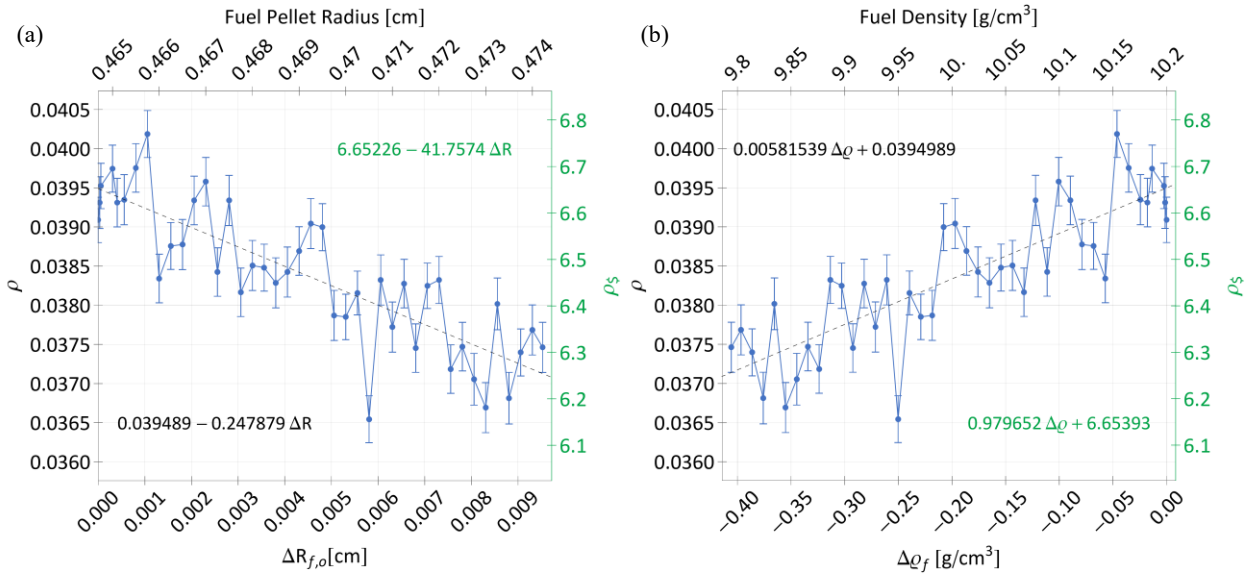

Figure 2-12. Reactivity as the (a) Radius and (b) Density of the UO_2 Fuel Changes with Thermal Expansion

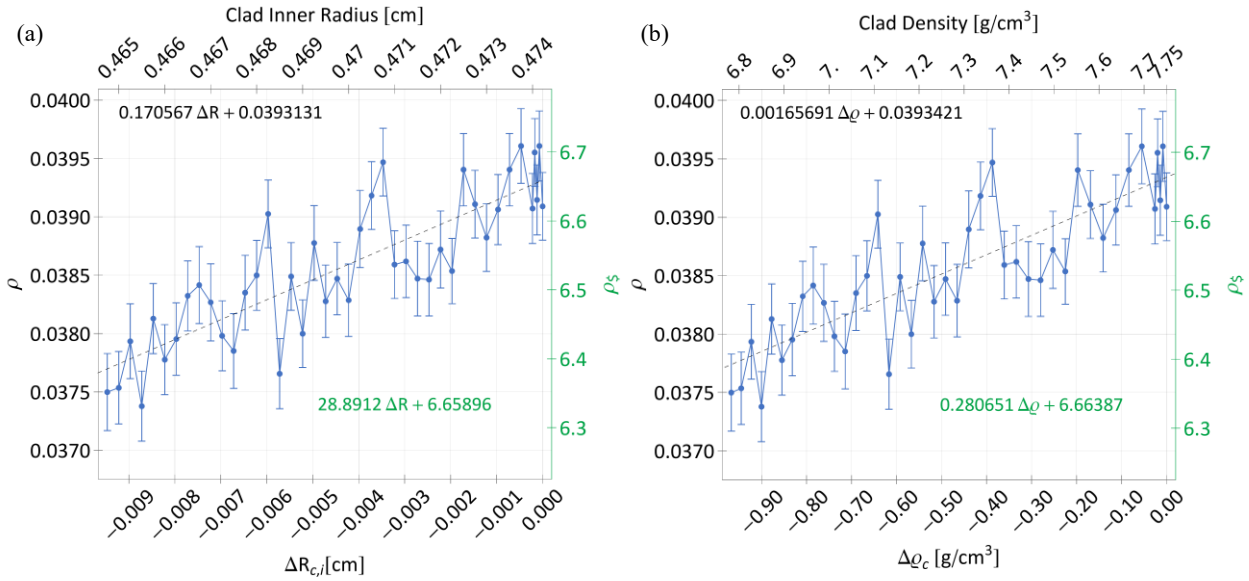

Figure 2-13. Reactivity as the (a) Inner Radius and (b) Density of the ZIRLO Clad Changes with Thermal Expansion

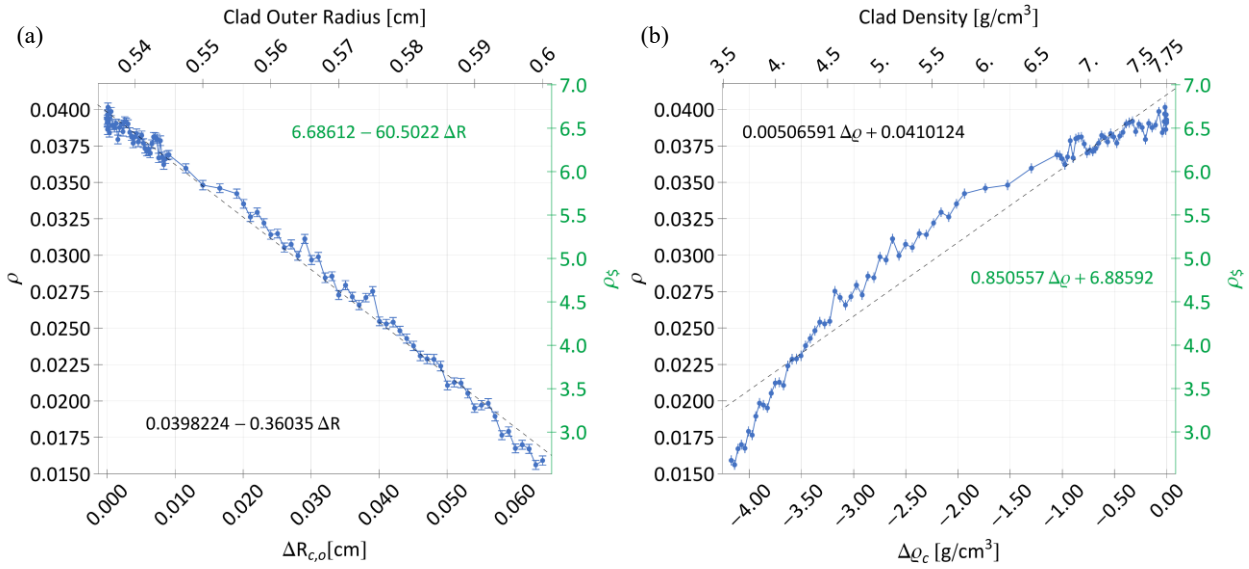

Figure 2-14. Reactivity as the (a) Outer Radius and (b) Density of the ZIRLO Clad Changes with Thermal Expansion

The reactivity feedback coefficients from the MCNP studies are summarized in Table 2-3. The definition of %void in RAZORBACK is the relative percent reduction in coolant density (g/cm^3), where the density of the saturated liquid was used for reference. The inner cladding radius study is used to provide the density feedback coefficient for the thermal expansion of ZIRLO as a byproduct.

Table 2-3. Feedback Coefficients Devised from MCNP Calculations Used in RAZORBACK

Mechanism	Coefficient	Units
Doppler Broadening in Fuel	$-0.082/\sqrt{T}$	\$/K
Relative Coolant Density Reduction	−0.285	\$/%void
Coolant Temperature	−0.011	\$/K
Fuel Thermal Expansion	−41.757	\$/cm
Fuel Density Changes	+0.980	$\$/(g/cm^3)$
Cladding Thermal Expansion – Outer	−60.502	\$/cm
Cladding Thermal Expansion – Inner	+28.891	\$/cm
Cladding Density Changes	+0.851	$\$/(g/cm^3)$

2.4.4 Kinetics of Water-Filled Clad Gap

Reactivity points for 90% B_4C/Al precipitation and above (Figure 2-6) were fitted to 4th-order polynomials and employed in RAZORBACK as piecewise time-dependent curves $\rho_\$(t)$ beginning at $\rho_\$ = \$0$. Reactivity insertions between \$1–\$3 are analyzed for periods of 10 milliseconds, 100 milliseconds, 500 milliseconds, 1 second, 5 seconds, and 10 seconds. Curves for the 1-second insertions are shown in Figure 2-15 as an example. In previous studies (Price et al. 2021), the reactivity insertion was modeled with space dependence as an analogy to reactor control rod movements (i.e., insertion and withdrawal). However, this type of reactivity insertion methodology was not representative of the progressive degradation states of the neutron absorber plates. Therefore, the time-dependent functions were employed instead.

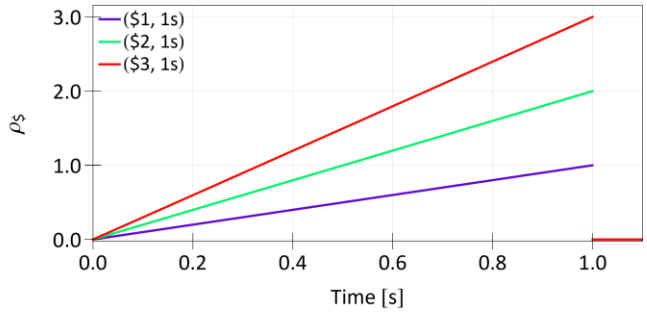

Figure 2-15. Piecewise Reactivity Curves for 1 second Insertions Fitted from the B_4C/Al Precipitation Results

The results for maximum power level and total integrated energy release observed during the transient are shown in Table 2-4 and Table 2-5, respectively. The 10 ms calculations did not complete because of closure of the clad gap from thermal expansion. This situation prevented negative feedback effects that would counteract the rapid progression of the energy release from being realized. Therefore, these results are highlighted in red. The power level of the successful runs ranges from approximately 10^7 W to 10^{10} W (with reference power of 10^6 W) while the energy ranges from 10^8 J to 10^9 J.

Reactivity feedback was driven primarily by the negative effect of Doppler broadening in the fuel. Feedback from the coolant had a small, lagging effect for the fast reactivity insertions; however, it became more significant for increasingly slower reactivity insertions, coming second in total effect for the 10-second calculations. This observation is linked to variation in coolant heating, which is determined by the thermal diffusivity of UO_2 and heat transfer from the clad surface. Thermal expansion in the UO_2 had more immediate effects compared to the cladding.

The maximum temperatures in the fuel, clad, and coolant channel are shown in Table 2-6, Table 2-7, and Table 2-8, respectively. These values represent observations during the transient, and it is plausible that the cladding and coolant temperatures may rise further upon termination of the event. The temperatures in the fuel and clad do not reach temperatures that would cause melting and loss of critical configuration; nonetheless, potential for cladding oxidation may need to be evaluated. The coolant temperatures rise above 100°C in some cases but do not exceed the boiling point based on the hydrostatic pressures of the water column modeled above the basket.

The temperatures do not appear to conform to a particular trend. Notably, among the successful runs, the 0.5-second datasets show elevated values of temperature for the fuel and cladding per given reactivity insertion as well as total energy release. This result suggests that that total energy release is not directly proportional to the magnitude of the reactivity insertion or rate, but rather it is due to other considerations including the relative timing of counteracting reactivity feedback effects (which are functions of location within the DPC) and heat transfer characteristics as influenced by the specific flow parameters. These nuances are worthy of further investigation, especially with respect the specific power profile modeled in the fuel.

Table 2-4. Maximum Power Level (W) of Transient

t (s)	$1	$2	$3
0.01	1.84E+11	9.50E+11	1.30E+12
0.1	3.93E+08	1.21E+10	3.11E+10
0.5	7.43E+08	2.02E+09	3.48E+09
1.0	2.49E+08	7.41E+08	1.36E+09
5.0	5.86E+07	8.65E+07	1.29E+08
10.0	2.65E+07	5.87E+07	1.18E+08

NOTE: Red shading indicates that the calculations did not complete because of cosure of the clad gap from thermal expansion.

Table 2-5. Total Energy Release (J) of Transient

t (s)	$1	$2	$3
0.01	2.60E+09	1.23E+09	1.02E+09
0.1	8.12E+08	1.02E+09	4.90E+08
0.5	1.12E+09	1.53E+09	1.43E+09
1.0	8.13E+08	1.12E+09	1.20E+09
5.0	7.22E+08	5.51E+08	7.66E+08
10.0	3.24E+08	7.22E+08	1.26E+09

NOTE: Red shading indicates that the calculations did not complete because of cosure of the clad gap from thermal expansion.

Table 2-6. Maximum Temperatures (°C) in the Fuel

t (s)	$1	$2	$3
0.01	1805.45	1191.75	922.03
0.1	796.82	1009.62	1163.46
0.5	1000.78	1241.68	1337.26
1.0	797.14	1001.89	1161.40
5.0	570.93	536.81	706.25
10.0	296.50	571.16	885.67

NOTE: Red shading indicates that the calculations did not complete because of cosure of the clad gap from thermal expansion.

Table 2-7. Maximum Temperatures (°C) in the Cladding

t (s)	$1	$2	$3
0.01	249.04	72.12	70.77
0.1	142.64	154.28	166.23
0.5	153.96	175.45	190.21
1.0	142.63	154.03	166.20
5.0	130.52	130.46	138.21
10.0	99.39	130.53	144.97

NOTE: Red shading indicates that the calculations did not complete because of cosure of the clad gap from thermal expansion.

Table 2-8. Maximum Temperatures (°C) in the Coolant

t (s)	$1	$2	$3
0.01	64.34	64.34	64.34
0.1	109.87	108.48	108.29
0.5	107.84	104.69	91.53
1.0	109.79	107.93	109.63
5.0	89.62	90.96	110.72
10.0	81.47	89.63	107.74

NOTE: Red shading indicates that the calculations did not complete because of cosure of the clad gap from thermal expansion.

2.5 Discussion

It has been demonstrated that reactivity insertions can be modeled in a transient analysis for a DPC given a reactivity insertion scenario involving the disintegration of neutron absorber plates. If corrosion products from the degraded absorbers settle (or are removed from solution) within a short time period, the resulting reactivity insertions could result in rapid releases of energy on the order of 10^8–10^9 J within a span of seconds. The credibility of such a transient occurring (i.e., reactivity insertion magnitude and rate) has not been evaluated for a specific repository and will be the subject of future work.

Results indicate that peak fuel temperatures do not rise to the extent that the SNF is damaged. The UO_2 fuel does not melt, and the ZIRLO cladding does not approach temperatures at which melting is possible, although cladding failure due to oxidation and pellet clad interactions at lower temperatures should be investigated further. Heat generation may result in localized boiling but will not expel the full volume of infiltrated water from the DPC. Doppler broadening is the dominant feedback mechanism for fast insertions, while additional effects from the coolant are evident for slow insertions.

The MCNP model can be improved by accommodating individual rod fidelity in the definition of temperature and density. This approach can support an assessment of the fission power distribution across the DPC, a study of power-peaking factors, and investigations of varying water levels in unsaturated geology. Also, the axial fission power distribution can be parametrized with respect to peaking along the active fuel length in a sensitivity study.

2.6 Continuing Work

Continuing work will refine understanding of reactivity insertion locations, rates, and magnitudes. The modeling framework is being expanded to an 89 BWR DPC with various assembly geometries (8×8, 9×9, and 10×10) for as-loaded configurations. Results will be compared with those from separate studies in fully saturated geology that will be described in Chapter 3.

The next phase of the analysis can apply the transient kinetics results to a solid mechanics study using a simplified DPC and barrier system. Software developed by Sandia National Labororatories such as SIERRA/SM and CTH can be used to investigate the effects of the transient criticality energy release on the stress field of the canister and surrounding materials.

This page is intentionally left blank

3. MODELING TRANSIENT CRITICALITY IN A SATURATED SHALE REPOSITORY

3.1 Description of Saturated Shale Repository

The geologic reference case for a hypothetical repository in saturated shale, or argillite, is illustrated in Figure 3-1. For this reference case, the repository is placed at a depth of 500 m, the emplacement drifts are backfilled with bentonite as a buffer (Mariner et al. 2017), and the waste package center-to-center spacing is 20 m (Hardin and Kalinina 2016). It is assumed that the hydrostatic pressure at repository depth is 50 bar. At this pressure, water boils at approximately 264°C (Weast and Astle 1979). Other characteristics of the host rock are given in Section 4.2.2 of Mariner et al. (2017).

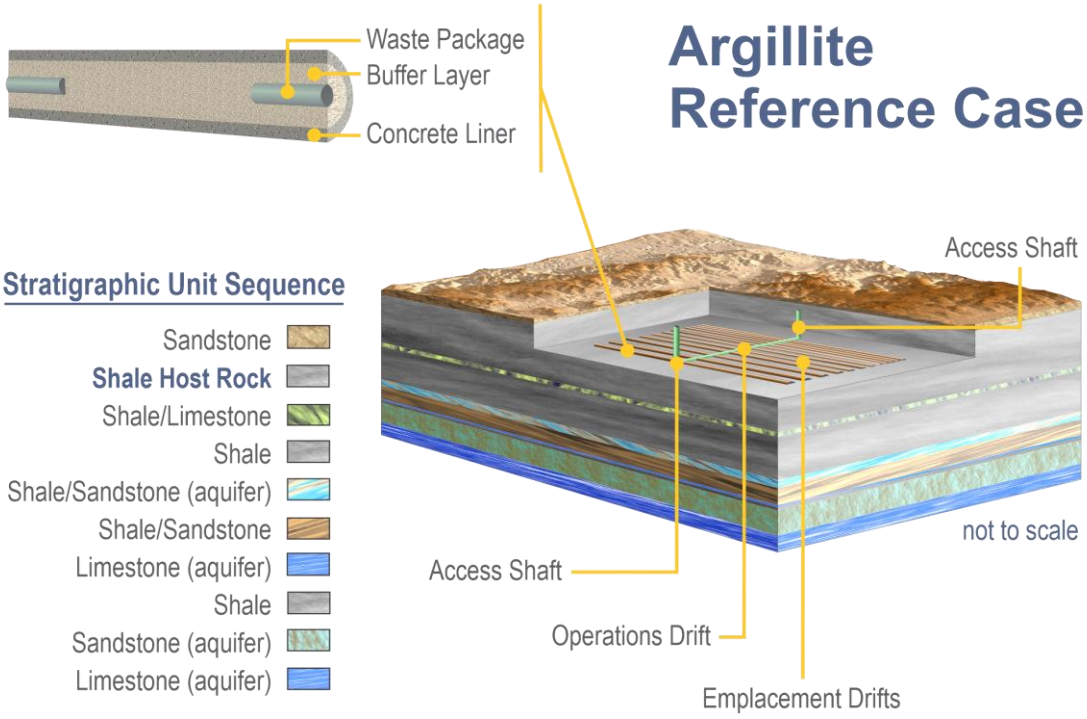

Figure 3-1. Conceptual Drawing of Hypothetical Reference Case for Saturated Shale/Argillite

3.2 Approach

The following subsections describe the approach taken to model a transient criticality event in a DPC disposed in a generic saturated shale repository.

3.2.1 Introduction and Background

A previous study was performed to evaluate the potential behavior of a transient criticality event in a DPC disposed in a shale saturated geologic repository containing PWR SNF (Price et al. 2021). For the study, the transient criticality event in the DPC was simulated through the rod ejection accident (REA) using the Studsvik Scanpower Inc. (Studsvik AB n.d.) SIMULATE-3K (S3K) code to evaluate characteristics such as peak power, duration, total energy released, and thermodynamic impacts during the power transient. The model focused on providing criticality transient characteristics based on the potential magnitudes and

rates of reactivity insertions as well as the reactivity feedback mechanisms. This REA analysis only considered the transient behavior from a localized reactivity insertion model. Therefore, this previous study was expanded to also simulate globalized reactivity insertion. This phenomenon was studied by first using the REA, with all control rods being uniformly ejected throughout the core, and then also through the boron dilution accident scenario.

In addition, a BWR DPC based on an MPC-89 containing General Electric (GE) BWR/4-6 fuel assemblies (8×8, 9×9, and 10×10) was evaluated to study similar behavior of a transient criticality event that was previously studied in the PWR DPC (Price et al. 2021).

3.2.2 Methodology Description

The study used Studsvik's S3K proprietary code (Studsvik AB n.d.) to perform the transient analysis for PWRs and BWRs. The first step was to develop the cross-sections input using CASMO, a lattice fuel 2D multigroup transport-based Method of Characteristics code (Grandi et al. 2011). The CASMO-generated files were then used for steady-state neutronic analysis in SIMULATE. The produced SIMULATE output includes steady-state nuclear analysis predictions, such as critical boron concentration, boron worth, reactivity coefficients, control rod worth, shutdown margin, power distributions, and peaking factors. Finally, these SIMULATE outputs were used in the thermal-hydraulics model of S3K to generate the transient neutronic analysis (Grandi et al. 2011).

3.2.3 PWR—Global Reactivity Insertion Analysis

The following subsections describe globalized reactivity insertion analysis performed for the PWR DPC using the REA and the boron dilution accident scenarios.

3.2.3.1 REA Analysis

A transient criticality event in a disposed DPC can potentially occur due to displacement of neutron absorbers or changes in geometry. To illustrate such a potential event, the REA can be used to simulate the mechanisms initiating a potential criticality transient event in the DPC. A REA in a reactor assumes rupture of the control rod drive mechanism, or of the control-rod-drive-mechanism nozzle. Upon this rupture, the pressure in the reactor coolant system provides an upward force that rapidly ejects the control rods from the core. The ejection of the control rods results in positive reactivity addition, leading to a peaked core power distribution. As the power rapidly rises, fission energy accumulates in the fuel rods faster than it can be transferred into the coolant, raising the fuel temperature. The power rise is mitigated primarily by fuel and moderator temperature reactivity coefficients.

The same methodology that was used to study the localized REA analysis was similarly used in the global reactivity insertion analysis (Price et al. 2021). The only difference is that all control rods are assumed to be uniformly ejected throughout the core. One scenario was evaluated at different reactivity insertion rates for approximately $2 reactivity worth.

3.2.3.2 Boron Dilution Accident Analysis

Another way to simulate global reactivity insertion into a DPC is to model a re-criticality accident condition in a reactor core. If the electrical power supply in a reactor is restored following the loss of electrical power, the emergency core cooling systems, and possibly also the feed water, would be activated and begin to inject unborated water into a PWR core. The increasing water level could cause re-criticality in the control rod-free part of the core.

An S3K model was developed to evaluate the re-criticality, through a potential reflooding, scenario. The cold-leg model, part of S3K functions, was used to initiate a boron dilution type transient from a steady state condition. Starting from zero power, the three cold legs begin to linearly reduce the soluble boron concentrations until it has reached zero. The boron distribution is applied in a time-dependent hydraulics calculation using a mapping of weighting factors.

3.2.4 BWR—Control Blade Ejection Accident Analysis

The BWR control blade ejection accident analysis is performed in the same manner as the PWR REA (Price et al. 2021). One difference between the PWR and BWR analysis is that the BWR control blades are inserted from the bottom to give a more homogenous distribution of the core power. Also, the BWR controls blades go between the fuel assemblies in the reactor core in such a way that four assemblies surround an inserted control blade.

3.2.4.1 Design Input

The DPC model is based on a BWR canister (MPC-89) without taking any credit for Metamic® material, which is assumed to degrade before the initiation of the transient. SNF assemblies irradiated in the Browns Ferry Power Plant are used. Figure 3-2 displays the layout of the fuel loading (initial enrichment [Enr] and maximum burnup [BU]) inside the DPC. The information was provided by Oak Ridge National Laboratory from the UNF-ST&DARDS (Clarity et al. 2017).

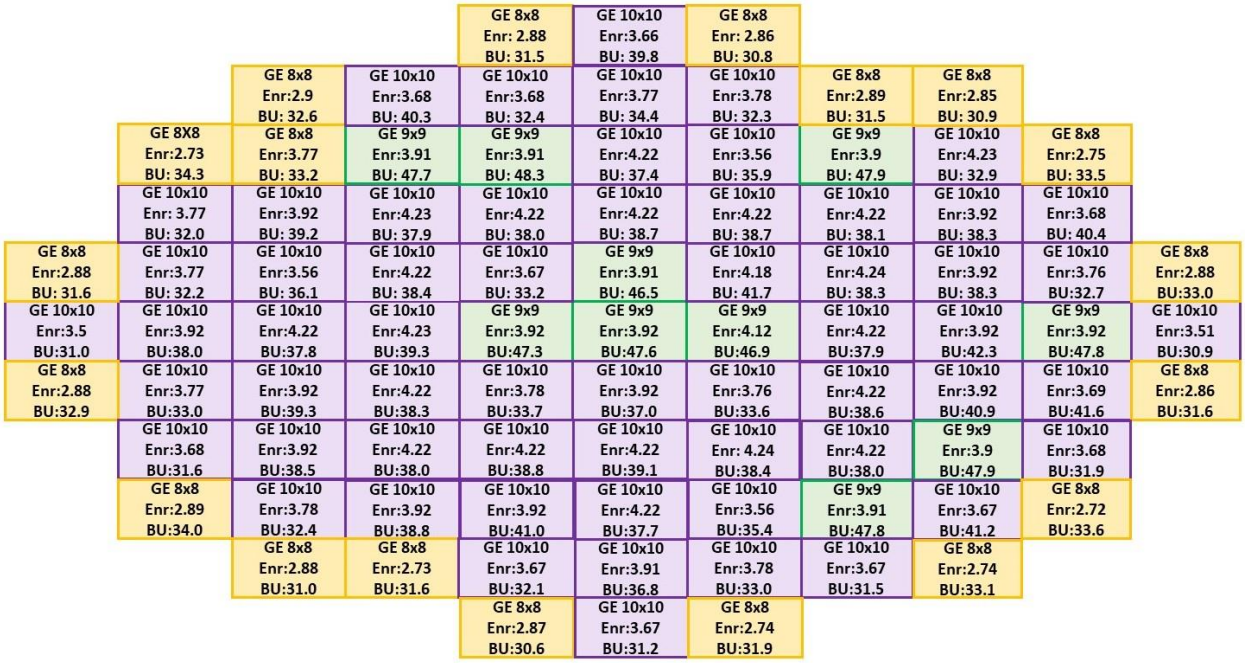

NOTE: BU = maximum burnup
Enr = initial enrichment

Source: Information from UNF-ST&DARDS.

Figure 3-2. Model Layout of MPC-89

The depletion characteristics of the GE 8×8, 9×9, and 10×10 BWR assemblies are shown in Table 3-1. The assembly layouts are shown in Figure 3-3, Figure 3-4, and Figure 3-5. The lattice positions mentioned in the figure notes are counted from the upper left corner of the figure. That is, the columns are numbered in increasing order in the negative *y* direction, while the rows are numbered in increasing order in the positive *x* direction.

Table 3-1. CASMO Input Depletion Parameters

Parameter	BWR 8×8	BWR 9×9	BWR 10×10
Assembly Pitch (cm)	15.24	15.24	15.24
Rod Pitch (cm)	1.62	1.45	1.30
Number of Fuel Rods	63	79	92
Number of Inert Rods	0	2	0
Type of Absorber/Poison	Gd	Gd	Gd
Number of Absorber Rods	5	7	14
^{235}U Enrichment/Poison (wt%)	3/3	3/3	3/5
^{235}U Enrichment (wt%)	~3 (Figure 3-3)	~4 (Figure 3-4)	~4 (Figure 3-5)
Active Fuel Length (cm)	381.0	381.0	381.0
Fuel Pellet Diameter (cm)	1.06	0.88	0.88
Fuel Temperature (K)	1200	1200	1200
Fuel Density (g/cm^3)	10.30	10.30	10.30
Specific Power (MW/MTU)	25	25	25
Moderator Temperature (K)	560.7	560.7	560.7
Moderator Density (g/cm^3)	varies axially, axial dependency	varies axially, axial dependency	varies axially, axial dependency

NOTE: BWR = boiling water reactor

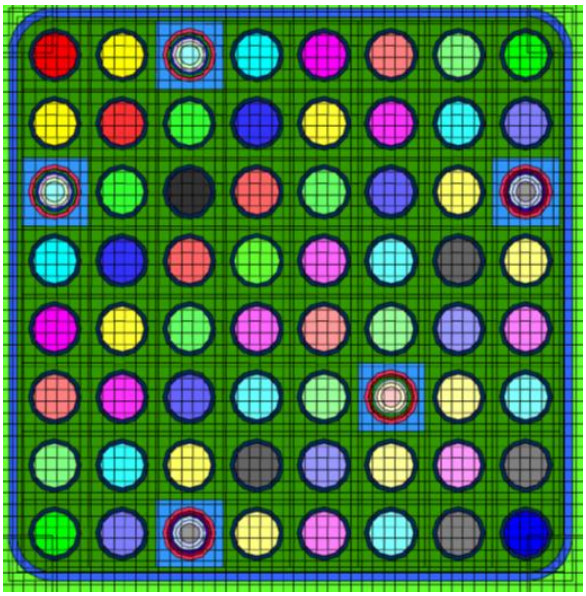

NOTE: The assembly has a water trap at lattice position (3, 3). There are five fuel-Gd rods (3 wt% Gd_2O_3) located in five fuel rod positions marked with multiple rings. Regular fuel pins are presented with a solid color and single outer ring (cladding).

Source: Information from UNF-ST&DARDS.

Figure 3-3. GE 8×8 Assembly Layout

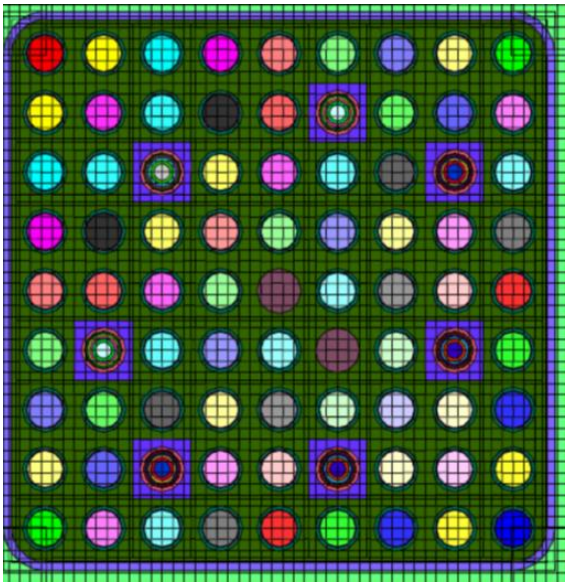

NOTE: The assembly has two inert rods at lattice positions (5, 5 and 6, 6). There are seven fuel-Gd rods (3 wt% Gd_2O_3) located in seven fuel rod positions marked with multiple rings. Regular fuel pins are presented with a solid color and single outer ring (cladding).

Source: Information from UNF-ST&DARDS.

Figure 3-4. GE 9×9 Assembly Layout

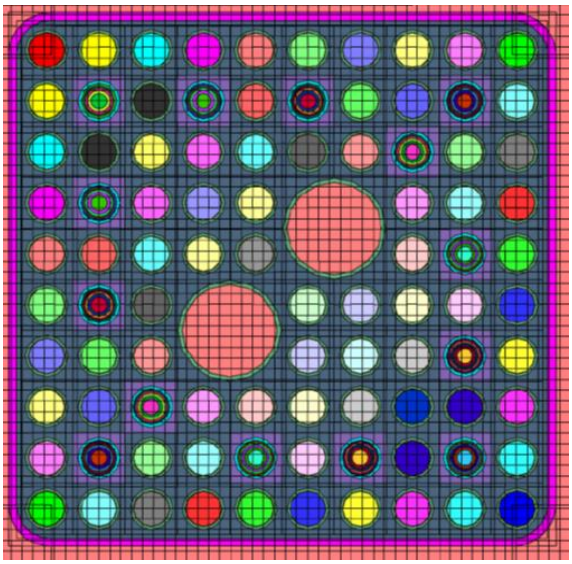

NOTE: The assembly has two water holes that occupy the following eight lattice positions: [(4, 6), (4, 7), (5, 6), (5, 7)] and [(6, 4), (6, 5), (7, 4), (7, 5)]. There are fourteen fuel-Gd rods (3 wt% Gd_2O_3) located in fourteen fuel rod positions marked with multiple rings. Regular fuel pins are presented with a solid color and single outer ring (cladding).

Source: Information from UNF-ST&DARDS.

Figure 3-5. GE 10×10 Assembly Layout

During the static and transient calculations, the DPC was modeled at a pressure of 725 psi at 0 m/s flowrate and 0 ppm soluble boron; these conditions are consistent with those for a saturated shale repository. The k_{eff} of the DPC is ~1.09; this value is an indication that the DPC has significant excess reactivity.

It should be mentioned that this k_{eff} value is lower than calculations performed by Oak Ridge National Laboratory, based on UNF-ST&DARDS, which produces a k_{eff} of ~1.19. The difference in values is mainly due to the difference in depletion assumptions (e.g., uniform moderator density, enriched fuel blanket). A test case was performed in CASMO/SIMULATE when the depletion characteristics were closely matched with UNF-ST&DARDS conditions. The k_{eff} values show that there is agreement between the Oak Ridge National Laboratory approach and the CASMO/SIMULATE analysis (Δk_{eff}~0.01).

3.2.4.2 Limitations/Assumptions

Since it is not the intended function of S3K to model transient analysis of canisters/out-of-reactor conditions, there are some limitations to the analysis. The following limitations apply:

- Control rod/blade movement is restricted based on design of the BWR and PWR reactor designs. That is, the control rods are inserted from the top in the PWR and are inserted from the bottom in the BWR.
- The maximum reactivity insertion rate (i.e., control rod withdrawal speed) is limited to 9,999 cm/s, which translates to 0.0365 seconds.
- CASMO/SIMULATE captures decay times on the order of tens of years and not the thousands of years (e.g., 9,000) that the DPC conditions require. This situation may make the isotopic

composition bounding in nature (i.e., higher excess reactivity in the DPC); the impact of isotopic changes during geologic disposal (e.g., decay of ^{240}Pu and ^{239}Pu) on transient and system kinetics will be the subject of future work. To capture the thermal effects of longer decay times, the fuel is modeled as cold, as the decay heat transfer model/option was turned off in S3K.

3.3 Results

3.3.1 PWR—Global Reactivity Insertion Analysis

The following subsections describe the results of the global reactivity insertion analysis for PWR DPC-37.

3.3.1.1 REA Results—Rod Ejection Accident

The PWR localized reactivity insertion study is compared to the global reactivity insertion scenario in Table 3-2. As can be seen from the results, similar behavior/values can be seen for moderator temperature while the fuel temperature was lower for the global reactivity insertion. Conversely, significant differences were noticed in the total energy released during the transient when the global reactivity insertion was higher than localized reactivity insertion. This situation occurs in part because the doppler effect provides stronger and faster feedback as a result of higher fuel temperature in the localized scenario compared to the global case. At the beginning of the transient, the core average moderator temperature is 450 K. The maximum average moderator temperature reached during the transient for all insertion times considered is approximately 471 K, indicating an increase of 21 K. The initial transient average fuel temperature is 447 K and the initial peak/maximum fuel temperature pretransient is 537 K. The maximum average fuel temperature reached during the transient is approximately 505 K, resulting in a maximum temperature increase of 58 K. The maximum/peak fuel temperature is about 912 K, indicating an increase of 375 K. Figure 3-6 shows the transient peak power versus time for the fastest insertion time considered (~0.04 seconds).

Table 3-2. Summary of Criticality Transient Results—Comparison of Localized versus Global Reactivity Insertion

Parameter	Insertion Time (s)			
	0.073	0.0365	0.073	0.0365
	Reactivity Worth			
	$1.8	$1.8	$2.2	$2.2
	Localized Reactivity Insertion		Global Reactivity Insertion	
Peak Power (MW)	2.37E+04	2.38E+04	7.32E+04	7.32E+04
Total Energy (MJ)	4.13E+03	2.21E+03	9.39E+04	9.17E+04
Maximum Fuel Temperature	692.1°C (965.2 K)	691.8°C (964.9 K)	639.3°C (912.4 K)	639.3°C (912.2 K)
Maximum Average Fuel Temperature	280.4°C (553.5 K)	280.3°C (553.4 K)	232.1°C (505.2 K)	232.1°C (505.2 K)
Maximum Water Temperature	411.8°C (684.9 K)	412.4°C (685.5 K)	407.7°C (680.8 K)	407.7°C (680.8 K)
Maximum Average Water Temperature	199.9°C (473 K)	200.3°C (473.4 K)	198.3°C (471.4 K)	198.3°C (471.4 K)
Transient Time (s)	0.59	0.59	0.21	0.21

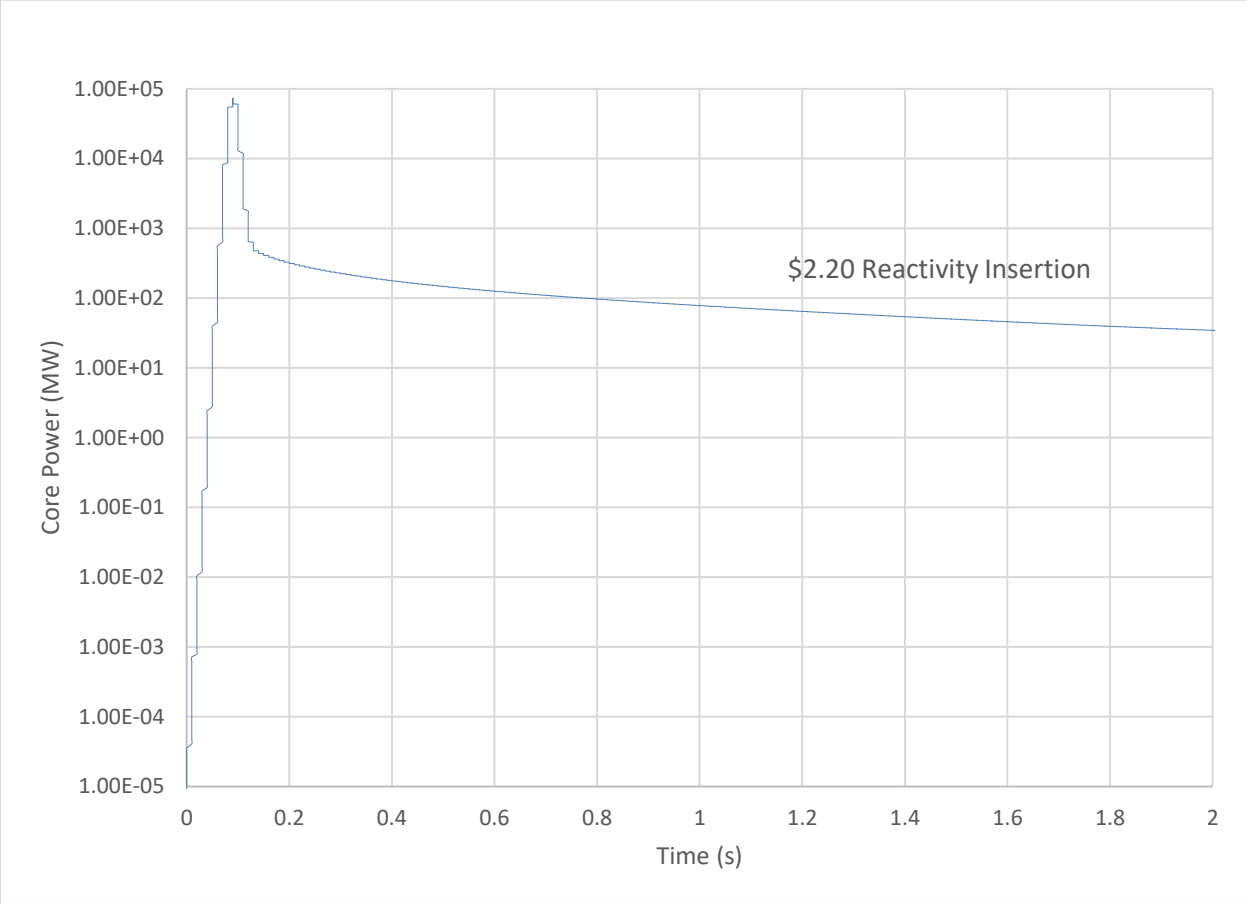

NOTE: Reactivity insertion time is ~0.04 seconds.

Figure 3-6. Transient Power versus Time for Global Reactivity Insertion Model—PWR

3.3.1.2 Boron Dilution Accident Results

Various modeling approaches were considered to attempt to simulate a criticality transient during DPC conditions at low core power and with no core flow. Due to the restricted DPC conditions when the flow rate is zero, only a minimally weak transient was observed. Therefore, no useable data was obtained. It can be concluded that this reactor accident scenario is not appropriate to evaluate criticality transients in a DPC environment.

3.3.2 BWR—Control Blade Ejection Accident Analysis

The following subsections provide the results of the control blade ejection accident analysis for BWR DPC-89.

3.3.2.1 Fuel Temperature Coefficient

Perturbations were performed to calculate the distributed Doppler coefficient as a function of the fuel average temperature in DPC modeled conditions. The method used calculates the reactivity change associated with a change in fuel temperature having the same spatial distribution as the power divided by the change in the average fuel temperature.

Table 3-3 presents the results from this method of the calculated Doppler coefficients as a function of fuel temperature. The results from the distributed Doppler coefficient reflect the power gradient/peaking in the DPC (shown in Table 3-5 and Table 3-6). The distributed Doppler coefficient is also illustrated in Figure 3-7.

Table 3-3. Distributed Doppler Coefficient in the DPC

Fuel Average Temperature (°C)	Fuel Average Temperature (°F)	Distributed Doppler Coefficient (pcm/°F)
10	50	−3.98
38	100	−3.63
66	150	−3.21
93	200	−2.86
121	250	−2.6
149	300	−2.47
177	350	−2.38
232	450	−2.28
260	500	−2.18
316	600	−2.11
371	700	−2.01
427	800	−1.95
482	900	−1.89
538	1,000	−1.8
649	1,200	−1.68
816	1,500	−1.57
982	1,800	−1.45
1,093	2,000	−1.34
1,371	2,500	−1.21
1,649	3,000	−1.14
1,927	3,500	−1.07
2,204	4,000	−1.03

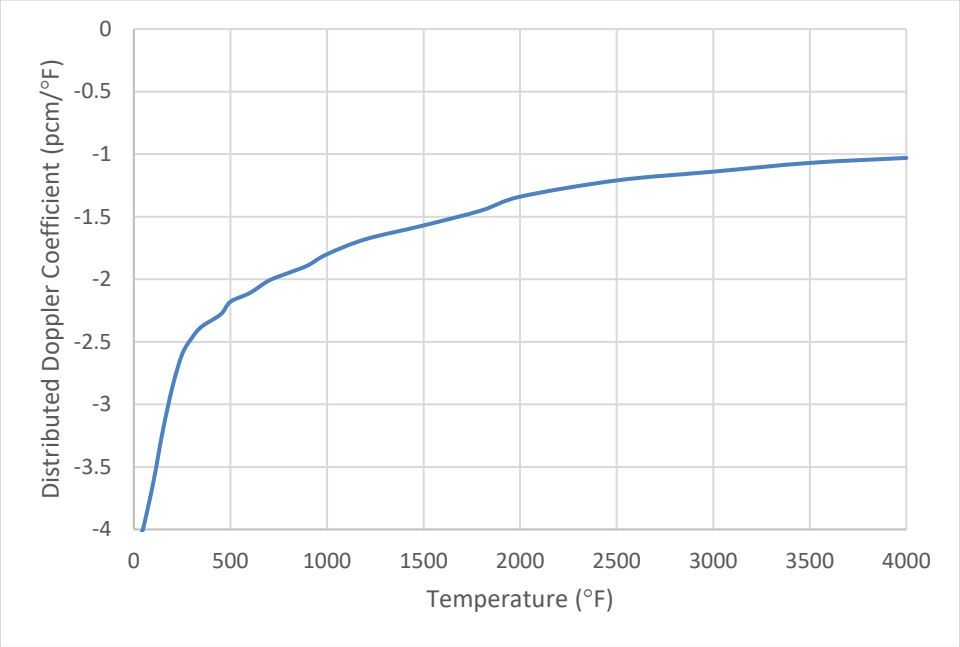

Figure 3-7. Distributed Doppler Coefficient

3.3.2.2 Moderator Temperature Coefficient

MTCs were calculated as a function of the coolant average temperature. The saturation temperature of the DPC at 725 psia is 507°F. The results are presented in tabular format in Table 3-4 and illustrated in Figure 3-8. The results show that the MTCs are positive at lower temperatures, indicating that the DPC is overmoderated at full density water. Also, in a comparison of the BWR MTCs to the PWR MTCs (Price et al. 2021), the BWR-produced values are less negative. This situation is potentially due to the higher ^{239}Pu concentration in the upper regions of BWR SNF (where the reactivity insertion occurs) compared to PWR SNF. In addition, there is a higher amount of neutron absorbers at the critical state (because there is significant excess reactivity in the BWR DPC), which might also affect the MTC since reduced moderation reduces fission and parasitic absorption concurrently. These noted trends and their potential mechanisms will be investigated further to better understand these results.

Table 3-4. Moderator Temperature Coefficients in the DPC

Coolant Average Temperature (°C)	Coolant Average Temperature (°F)	MTC (pcm/°F)
13	55	2.4
41	105	1.9
68	155	0.6
96	205	−0.4
124	255	−1.2
152	305	−2.0
179	355	−3.6
207	405	−5.2
235	455	−7.1
263	505	−8.9

NOTE: MTC = moderator temperature coefficient

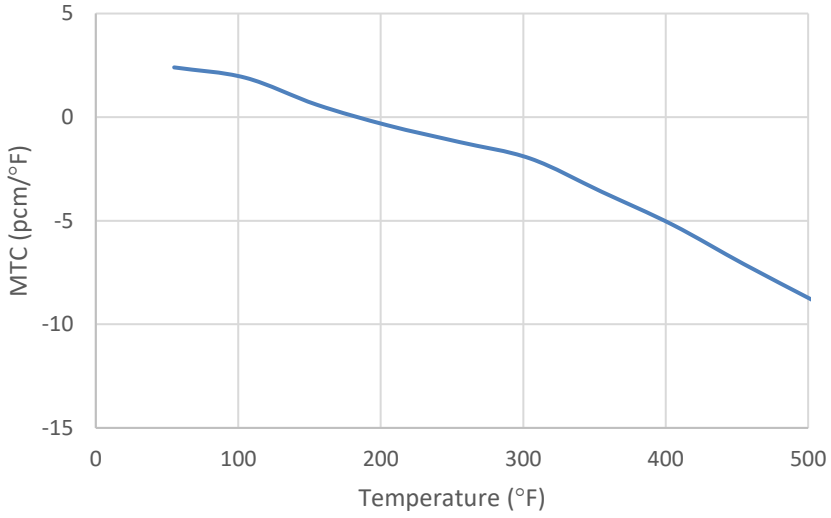

Figure 3-8. Moderator Temperature Coefficient

3.3.2.3 Control Blade Ejection Accident Results

Summaries of the transient criticality scenarios are presented in Table 3-5 and Table 3-6. The summaries include peak power of criticality transient, total energy released during criticality transient, duration of criticality transient, fuel temperature, moderator temperature, and peaking factors. The reactivity insertion magnitudes are evaluated around $1.2 and $3.2. Five different reactivity insertion times are considered ranging from approximately 0.04 seconds to 7 seconds.

Table 3-5 presents the reactivity insertion at \$1.20 as a function of reactivity insertion time. The results indicate that the two slowest insertion times considered (~7 seconds and ~ 2 seconds) do not fully complete the transient before all of the reactivity worth has been inserted (i.e., the control blades/rods have not been fully withdrawn during the transient). The highest peak power (3.40E+02 MW) occurs during the two fastest insertion times, which also corresponds to the largest amount of energy released (~3.0E+02 MJ). The maximum average moderator temperature reached during the transient for all insertion times considered is approximately 523 K. It should be noted that the maximum moderator temperature occurs when the transient has reached near-pretransient power levels, a time much past the end of the transient (i.e., after the DPC has reached a subcritical state).

Table 3-5 shows that maximum average fuel temperature reached during the transient for all insertion times considered is approximately 516 K. The maximum/peak fuel temperature is about 837 K for all insertion times considered. These results demonstrate that the fuel would likely remain intact during the transient as the peak temperature is far from the melting temperature (about 3,000 K for UO_2). While not included in the results in Table 3-5, the surface temperature of the fuel rod indicates that the cladding remains intact given that the cladding temperature would be comparable to the surface temperature of the fuel rod.

As a side note, the core inlet and exit temperatures remain unchanged during the transient confirming that the no-flow conditions in the DPC have been captured.

Table 3-5. Summary of Criticality Transient Results—Reactivity Insertion Amount \$1.20

Reactivity Insertion Amount \$1.20					
Parameter	**Insertion Time (s)**				
	7.3[a]	**1.825[b]**	**0.9125**	**0.073**	**0.0365**
Peak Power (MW)	2.40E+02	2.80E+02	2.16E+03	3.40E+02	3.40E+02
Total Energy (MJ)	4.55E+02	3.96E+02	3.44E+02	2.99E+02	2.96E+02
Maximum Fuel Temperature	501.85°C (775 K)	544.85°C (828 K)	559.85°C (833 K)	563.85°C (837 K)	563.85°C (837 K)
Maximum Average Fuel Temperature	206.85°C (480 K)	237.85°C (511 K)	240.85°C (514 K)	242.85°C (516 K)	242.85°C (516 K)
Maximum Water Temperature	255.85°C (529 K)	255.85°C (529 K)	255.85°C (529 K)	255.85°C (529 K)	255.85°C (529 K)
Maximum Average Water Temperature	246.85°C (520 K)	248.85°C (522 K)	249.85°C (523 K)	249.85°C (523 K)	249.85°C (523 K)
Transient Time (s)	2.62	1.20	0.98	0.82	0.81
Power Peaking Factor	1.93	1.93	1.93	1.93	1.93

NOTE: [a] Insertion time too slow for transient; reactivity insertion ~ \$1.0.
[b] Insertion time too slow for transient; reactivity insertion ~ \$1.1.

The results from the highest reactivity insertion (\$3.20) are presented in Table 3-6 as a function of reactivity insertion time. The majority of the insertion times considered were not sufficiently quick for the transient to fully complete before all of the reactivity worth has been inserted (i.e., the control blades/rods have not been fully withdrawn during the transient). Consistent with previously presented results

(Table 3-5), the highest peak power (3.29E+04 MW) occurs during the two fastest insertion times, while the largest amount of energy (3.49E+03 MJ) is released during the 0.07-second insertion time. The maximum average moderator temperature reached during the transient for all insertion times considered is approximately 532 K.

The maximum average fuel temperature, displayed in Table 3-6, reached during the transient for all insertion times considered is approximately 685 K. The maximum/peak fuel temperature reached during the transient is about 1,685 K. While these fuel temperature increases are significantly larger than those observed for previous transients (Table 3-5), the fuel would likely remain intact during this higher reactivity transient as the peak temperature is far from the melting temperature; however, potential cladding failure would have to be evaluated.

Another observation is that the transient duration is shorter than previous results have indicated for all insertion times.

Table 3-6. Summary of Criticality Transient Results—Reactivity Insertion Amount $3.20

Reactivity Insertion Amount $3.20					
Parameter	**Insertion Time (s)**				
	7.3[a]	**1.825[b]**	**0.9125[c]**	**0.073**	**0.0365**
Peak Power (MW)	8.00E+02	2.25E+03	5.30E+03	3.29E+04	3.28E+04
Total Energy (MJ)	5.43E+02	1.22E+03	2.26E+03	3.49E+03	3.45E+03
Maximum Fuel Temperature	571.85°C (845 K)	746.85°C (1,020 K)	910.85°C (1,184 K)	1,411.85°C (1,685 K)	1,411.85°C (1,685 K)
Maximum Average Fuel Temperature	246.85°C (520 K)	264.85°C (538 K)	315.85°C (589 K)	411.85°C (685 K)	411.85°C (685 K)
Maximum Water Temperature	261.85°C (535 K)	261.85°C (535 K)	261.85°C (535 K)	261.85°C (535 K)	261.85°C (535 K)
Maximum Average Water Temperature	251.85°C (525 K)	253.85°C (527 K)	255.85°C (529 K)	258.85°C (532 K)	258.85°C (532 K)
Transient Time (s)	0.6	0.27	0.18	0.07	0.07
Power Peaking Factor	1.98	1.98	1.98	1.98	1.98

NOTE: [a] Insertion time too slow for transient; reactivity insertion ~$1.2.
[b] Insertion time too slow for transient; reactivity insertion ~$1.6.
[c] Insertion time too slow for transient; reactivity insertion ~$1.9.

Figure 3-9 shows the transient peak power of $3.20 reactivity insertion for the fastest reactivity insertion rate considered (~0.04 seconds). This highest reactivity insertion transient begins to decrease at a faster rate in power after the completion of the peak transient (i.e., once k_{eff} reaches ~0.999) and eventually returns to the pretransient power level.

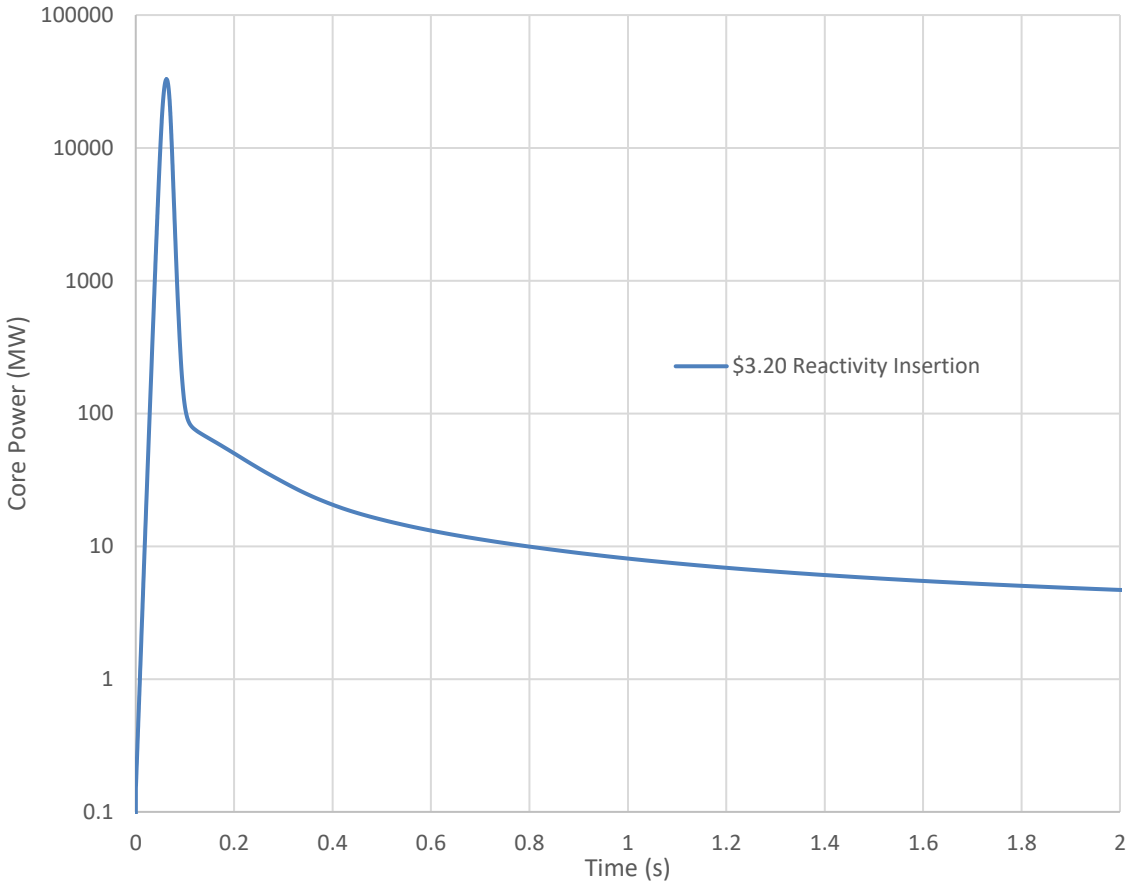

Figure 3-9. Transient Power versus Time—BWR

4. SUMMARY, CONCLUSIONS, AND FUTURE WORK

The rising number of DPCs being used to store commercial SNF has prompted interest in the possibility of direct disposal of DPCs in a geologic repository. Since DPCs were designed for temporary storage rather than permanent disposal, research is being conducted regarding the potential behavior of DPCs and their contents under repository conditions. In evaluating the long-term performance of a repository, one of the events that may need to be considered is the SNF achieving a critical configuration. A key challenge is the need to create the modeling tools and techniques that may eventually be required to either exclude criticality from or include criticality in a PA as appropriate.

A multiyear effort has been initiated to examine the potential consequences of criticality events with respect to long-term repository performance. The research effort began with a scoping phase to develop an approach to creating the needed modeling tools and techniques (Price et al. 2019a) followed by a second phase consisting of initial implementation of the approach and identification of future work (Price et al. 2019b). In the subsequent study, the research team considered relevant FEPs and moved forward with the development of modeling capabilities (Price et al. 2021). The work on modeling steady-state criticality considered multiple canisters in a repository-scale PA while the work on modeling transient criticality focused on a single canister under repository conditions.

This report marks the second iteration of work on the development of transient criticality modeling capabilities. The transient criticality modeling applies to the case in which the approach to criticality (reactivity insertion) is fairly rapid, causing the k_{eff} to overshoot the value of unity leading to an (initially) exponential increase in power that is coupled to thermal and mechanical effects, until the negative feedback mechanisms cause the k_{eff} to drop back below unity. The neutronic, kinetic, and thermal-hydraulic processes important to evaluating transient criticality and its potential adverse impacts on repository performance are examined. Output parameters of interest include peak power, total energy, fuel temperature, and water temperature over the course of the simulated transient criticality.

The focus is on the consequences of criticality, not the probability of occurrence of criticality, though the latter is a topic planned for investigation in the future. In addition, the scope is limited to in-package criticality in DPCs; external criticality has not been examined. The study team considered two different geologic reference cases for generic repositories: an unsaturated alluvium repository (Section 2) and a saturated shale repository (Section 3).

4.1 Summary and Conclusions

4.1.1 Unsaturated Alluvium Repository

The transient criticality analysis in an unsaturated alluvium repository has benefitted from evolving technical improvements since the last iteration documented in Price et al. (2021). In the previous report, emphasis was placed on characterizing reactivity in basic degradation states of the canister, characterizing reactivity feedback for a fully inundated void volume, and providing an initial demonstration of the kinetics approach that integrated results from neutronics.

This iteration of the study has shown significant progress in the development of the MCNP model to include a partial water level to account for both water and air across all void space in the DPC. The reactivity insertion scenario has been refined to correspond to neutron absorber plate degradation driven by exposure to infiltrated groundwater, and it has been implemented in the kinetics study as a time-dependent reactivity insertion as opposed to a spatially dependent insertion (like a control rod). The material inventory obtained from UNF-ST&DARDS features 18-node axial fidelity as opposed to the homogenous inventory smeared across each assembly employed in the last study.

Reactivity feedback coefficients were re-evaluated for this detailed inventory and, upon further inspection of the code documentation, the fit of the coolant voiding coefficient was revised using specialized units required by RAZORBACK. The kinetics analysis was performed with refined dimensions, including the use of prototypic-length fuel and coolant channels representative of the head space above and below the fuel in the basket. The fission power profile was implemented as a polynomial approximation of results obtained from CINDER for the central assembly slot in a 37 PWR basket. This distribution conformed to a Gaussian or exponentially modified Gaussian, while the study in the last report used a parabolic distribution nearly symmetric about the center of the fuel element.

The updated transient analysis demonstrated that, for reactivity insertions between \$1 and \$3 and various insertion rates, the resulting power pulses did not lead to temperatures in the fuel or cladding that would compromise fuel geometry or lead to conditions susceptible for rapid zirconium oxidation. The magnitudes of the energy releases were on the order of 10^8 – 10^9 J, which is on par with previous investigation in Price et al. (2021). The maximum observed temperatures in the fuel and cladding did not conform to a trend based on the insertion characteristics, which suggests time-dependent effects from the relative timing of counteracting reactivity feedback effects as well as spatial variation in the heat-transfer conditions. Like before, RAZORBACK was unable to completely evaluate the rapid reactivity insertions occurring over a 10-millisecond period, although this issue may be addressed with further development. Altogether, further refinement in the kinetics study is suggested before using the results in solid mechanics studies for the DPC. These refinements are discussed in Section 4.2.1.

4.1.2 Saturated Shale Repository

Price et al. (2021) considered the potential behavior of a transient criticality event in a DPC disposed in a shale saturated repository containing PWR SNF. The transient criticality event was simulated using the REA analysis capability in S3K to evaluate characteristics such as peak power, duration, total energy released, and thermodynamic impacts during the power transient. Because this previous study only considered the transient behavior from a localized reactivity insertion model, the work presented in Section 3 expanded the previous effort to also simulate globalized reactivity insertion using the REA and boron dilution accident scenarios. In addition, a BWR DPC based on an MPC-89 containing GE 8×8, 9×9, and 10×10 assemblies was evaluated for comparison with similar studies involving the PWR DPCs.

The following conclusions can be drawn based on simulations of criticality transients with reactivity insertions up to \$3.20 in the DPC using the reactor core transient analysis code S3K:

- **PWR Local versus Global Reactivity Insertions**—The PWR global reactivity insertion model showed a lower peak fuel temperature compared to the localized PWR reactivity insertion model. Conversely, the total energy released during the transient for the global reactivity insertion was higher than the localized reactivity insertion, which also resulted in a higher peak power. This result is in part due to the doppler effect providing stronger and faster feedback because of higher fuel temperature in the localized scenario compared to the global case.
- **PWR versus BWR Local Reactivity Insertion**—It was observed that the BWR localized reactivity insertion models produced overall lower peak powers and total energy released. In addition, higher peaking factors compared to the equivalent reactivity transient PWR model were also noted. These trends may be attributed to differences in composition of the fuel for the location of transient, which is at the top for the BWR assemblies (higher ^{239}Pu concentration) versus the bottom for the PWR assemblies (lower ^{239}Pu concentration). These composition differences and their impacts on the transients will be the subject of future studies.

4.2 Future Work

4.2.1 Unsaturated Alluvium Repository

For transient criticality studies in unsaturated alluvium, the feedback study with MCNP must examine thermal scattering effects (S[α,β]) associated with temperature changes in the moderator. Generally, further inspection is required to improve the quality of fit for the moderator feedback results.

Development tasks for the RAZORBACK source code are intended to support the novel application of the program to the disposal context. Given that the code was originally devised to model reactivity insertion characteristics for engineered research reactors, there are several considerations for establishing modeling parity in the repository context. Software development can assist in closing technical gaps and improving quality of the final results. Source code inspection can illuminate issues observed with heat transfer and the water equation of state and remove limitations that have hindered successful completion of simulations, especially with greater reactivity insertions.

Modifications are needed to address several considerations for a horizontally emplaced canister system. Representation of the hydrostatic pressure head in the DPC would include variation in the radial direction as opposed to the axial direction. For a given fuel element, this difference would remove an unnecessary (and unrealistic) spatial dependency in the heat transfer characteristics of the coolant as the water density would be axially uniform prior to the transient.

Given the time scale of the transient, recharge from groundwater seepage through a canister breach is not expected to introduce active flow into the system. Therefore, heat transfer in the DPC would be determined by conduction, natural convection, and boiling. A natural convection heat transfer correlation for horizontal SNF assemblies can be applied to the governing equations as opposed to the default models for vertical flow. Within the SFWST scope of activities, there are opportunities to incorporate horizontally oriented and SNF-specific correlations for Nusselt and Grashof numbers derived from scaled test data or field measurements.

With regards to other heat transfer-related concerns, inspection may be needed for portions of the specific heat and thermal conductivity curves included for UO_2 and Zircaloy. It is not clear whether the piece-wise functions for these thermophysical properties, which are needed to define behavior leading up to the melting point, are responsible for numerical errors during program execution. Inspection of the two-phase transition for water is also needed, with emphasis on the role of certain parameters in the input deck (in particular the boiling expansion suppression factor) that influence the treatment of the saturated zone. Expansion of output fidelity for temperatures, particularly the thermal profile in the fuel, can improve the quality of final results. An additional feature slated for development would include proper accommodation of nonlinear reactivity feedback behavior from coolant voiding.

As discussed in Section 2.4.2, the fission power profile, as evaluated from a depletion code for the 22,000-year inventory, conforms mostly to a Gaussian profile and is characteristic of SNF as opposed to profiles expected in a pulsed reactor. The source code must be modified to accommodate this functional form apart from the default 6^{th}-order polynomial convention, which is inaccurate at representing the depletion results. Additional attention would be required in curve-fitting to ensure proper normalization.

The definition of time-dependent reactivity insertions can be enhanced with a higher-order polynomial or alternative functional form (e.g., exponential). Source code inspection is also needed for cases in which reactivity was observed to increase (likely from positive reactivity effects from coolant pressure fluctuations) after the user-defined insertion end time. If the spatially dependent reactivity insertion (as

imparted from the control rod mechanisms) is revisited for modeling the B_4C/Al degradation, the feature can be improved by adding alternative functional forms apart from the default sine-squared fit.

The sum of various improvements to the kinetics methodology will increase the quality and consistency of final results for transient pulse power output, energy release, and temperature evolution. Once these phenomena are well characterized, the transient energy release evaluated in RAZORBACK can be applied as the source term for hydrosimulations of the resulting shock wave in the unsaturated void space of the DPC. Solid-mechanics simulations can be performed to evaluate the canister and EBS integrity given the stress field resulting from the transient criticality event. Additionally, given that this analysis was restricted to a 37 PWR DPC, a parallel study can be conducted for an 89 BWR DPC with an as-loaded configuration of assembly inventories. Results can be compared based on characteristics that are likely to arise from differences in the SNF, for example, the fission power profile being representative of the specialized loading of BWR fuel rods and corresponding power operation characteristics.

4.2.2 Saturated Shale Repository

To advance development of transient criticality modeling capabilities in a saturated shale repository, it is recommended that the following topics for PWR and BWR DPCs be investigated further:

- **Impact of Decay on Transients**—As SIMULATE/S3K is limited in the length of cooling/decay time, changing the fuel composition through isotopic manipulation would more accurately represent fuel composition/isotopic concentrations at 9,000 + years decay time. This approach could be bounded by (1) evaluating only the presence of uranium isotopes (^{235}U), zeroing out plutonium (^{239}Pu) influence, and (2) evaluating only plutonium (^{239}Pu).
- **Impact of Axial and Radial Insertion Location on Transients**—As the results for both the PWR and BWR DPCs show that there is significant power peaking in the DPC because of the loading pattern, it would be beneficial to further study reactivity insertion locations at various positions in the DPC.
- **Impact of Assembly Design, Initial Enrichments, Burnup, and DPC Loading on Transients**—To ensure representative DPCs have been selected for the transient criticality analysis, additional assembly designs featuring varied initial enrichments and burnups should be considered for investigation and comparison with these results.
- **Impact of DPC Orientation on Analysis Models**—SIMULATE/S3K models a vertical flooded core, whereas the DPC will likely initially be in a horizontal orientation and would be potentially flooded along the length of fuel assemblies (as opposed to height). This flooding configuration could impact the relatively slower criticality transient behavior, especially if convective heat transfer in the moderator becomes important for the determination of the MTC.
- **Impact of Water Composition**—Impurities in water can potentially harden the spectrum. Water present in the DPC could become contaminated over time with dissolved species as neutron absorbers and baskets degrade. Additionally, this condition may result in an initial positive MTC, similar to that of a PWR reactor at the beginning of the cycle due to the high soluble boron concentration.
- **Evaluation of the Potential for and Behavior of Secondary Transient Pulses**—There is a possibility that the initial transient pulse can be followed by subsequent secondary transient pulses, which would result in a higher total energy release. Further studies should be carried out to evaluate the impact of any potential secondary pulses on the DPC.

5. REFERENCES

10 CFR 63. *Disposal of High-Level Radioactive Wastes in a Geologic Repository at Yucca Mountain, Nevada.*

10 CFR 71. *Packaging and Transportation of Radioactive Material*.

10 CFR 72. *Licensing Requirements for the Independent Storage of Spent Nuclear Fuel, High-level Radioactive Waste, and Reactor-related Greater than Class C Waste*.

40 CFR 197. *Public Health and Environmental Radiation Protection Standards for Yucca Mountain, Nevada.*

73 FR 61256. *Public Health and Environmental Radiation Protection Standards for Yucca Mountain, Nevada.*

Bell, I.H., J. Wronski, S. Quoilin, and V. Lemort. 2014. Pure and Pseudo-pure Fluid Thermophysical Property Evaluation and the Open-Source Thermophysical Property Library CoolProp. *Industrial & Engineering Chemistry Research* 53 (6): 2498–2508. doi: 10.1021/ie4033999.

Briggs, J.B., L. Scott, and A. Nouri. 2003. The International Criticality Safety Benchmark Evaluation Project. *Nuclear Science and Engineering* 145 (1): 1–10.

Clarity, J.B., K. Banerjee, H.K. Liljenfeldt, and W.J. Marshall. 2017. As-Loaded Criticality Margin Assessment of Dual-Purpose Canisters Using UNF-ST&DARDS. *Nuclear Technology* 199:245–275. https://doi.org/10.1080/00295450.2017.1361250.

Cullen, D.E. and C.R. Weisbin. 1976. Exact Doppler Broadening of Tabulated Cross Sections. *Nuclear Science and Engineering* 60 (3): 199–229. doi: 10.13182/NSE76-1.

DOE (Department of Energy). 2008a. *Yucca Mountain Repository License Application*. DOE/RW-0573, Rev. 0. Las Vegas, NV: US Department of Energy, Office of Civilian Radioactive Waste Management.

DOE. 2008b. *Yucca Mountain Repository License Application*. DOE/RW-0573, Rev. 1. Las Vegas, NV: US Department of Energy, Office of Civilian Radioactive Waste Management.

Goorley, T. 2014. *MCNP6.1.1-Beta Release Notes*. LA-UR-14-24680. Los Alamos, NM: Los Alamos National Laboratory.

Grandi, G.M., K.S. Smith, J.D. Rhodes, III. 2011. *SIMULATE-3K Models and Methodology.* SSP9813r7. Studsvik Scandpower, Inc. (proprietary document).

Hardin, E. and E. Kalinina. 2016. *Cost Estimation Inputs for Spent Nuclear Fuel Geologic Disposal Concepts*. SAND2016-0235. Albuquerque, NM: Sandia National Laboratories.

Hardin, E., L. Price, E. Kalinina, T. Hadgu, A. Ilgen, C. Bryan, J. Scaglione, K. Banerjee, J. Clarity, R. Jubin, V. Sobes, R. Howard, J. Carter, T. Severynse, and F. Perry. 2015. *Summary of Investigations on Technical Feasibility of Direct Disposal of Dual-Purpose Canisters*. FCRD-UFD-2015-000129, Rev. 0; SAND2015-8712R. Albuquerque, NM: Sandia National Laboratories. doi: 10.2172/1504860.

Humphries, L.L., V.G. Figueroa, M.F. Young, D. Louie, and J.T. Reynolds. 2015. *MELCOR Computer Code Manuals*. SAND2015-6692R. Albuquerque, NM: Sandia National Laboratories.

Mariner, P.E., E.R. Stein, J.M Frederick, S.D. Sevougian, and G.E. Hammond. 2017. *Advances in Geologic Disposal System Modeling and Shale Reference Case*. SFWD-SFWST-2017-000044; SAND2017-10304R. Albuquerque, NM: Sandia National Laboratories.

Mariner, P.E., E.R. Stein, S.D. Sevougian, L.J. Cunningham, J.M Frederick, G.E. Hammond, T.S. Lowry, S. Jordan, and E. Basurto. 2018. *Advances in Geologic Disposal Safety Assessment and an Unsaturated Alluvium Reference Case*. SFWD-SFWST-2018-000509; SAND2018-11858R. Albuquerque, NM: Sandia National Laboratories.

Martin, W. 2012. *Implementation of On-the-Fly Doppler Broadening in MCNP5 for Multiphysics Simulation of Nuclear Reactors*. NEUP 10-897. Ann Arbor, MI: Battelle Energy Alliance.

Munro, R.G. 2002. *Elastic Moduli Data for Polycrystalline Ceramics*. NISTIR 6853. Gaithersburg, MD: National Institute of Standards and Technology.

Nuclear Waste Policy Act of 1982. 42 U.S.C. 10101 et seq.

OECD (Organisation for Economic Co-operation and Development) Nuclear Energy Agency. 2016. *Reactivity-Initiated Accident Fuel-Code Benchmark Phase II Volume 2: Task No. 1 Specifications*. NEA/CSNI/R(2016)6/VOL2. Paris, France: Organisation for Economic Co-operation and Development Nuclear Energy Agency.

Price, L.L., A. Salazar, E. Basurto, A.A. Alsaed, J. Cardoni, M. Nole, J. Prouty, C. Sanders, G. Davidson, M. Swinney, S. Bhatt, E. Gonzalez, B. Kiedrowski. 2021. *Repository-Scale Performance Assessment Incorporating Postclosure Criticality*. SAND2022-7932 R. Albuquerque, NM: Sandia National Laboratories.

Price, L.L., A.A. Alsaed, A. Barela, P.V. Brady, F. Gelbard, M.B. Gross, M. Nole, J.L. Prouty, K. Banerjee, S. Bhatt, G. G. Davidson, Z. Fang, R. Howard, S.R. Johnson, S.L. Painter, M. Swinney, E. Gonzalez. 2019b. *Preliminary Analysis of Postclosure DPC Criticality Consequences*. M2SF-20SN010305061; SAND2020-4106. Albuquerque, NM: Sandia National Laboratories.

Price, L.L., A.A. Alsaed, P.V. Brady, M.B. Gross, E.L Hardin, M. Nole, J.L. Prouty, K. Banerjee, and G.G. Davidson. 2019a. *Postclosure Criticality Consequence Analysis – Scoping Phase.* M3SF-19SN010305061; SAND2019-4644R. Albuquerque, NM: Sandia National Laboratories.

Spriggs, G., J. Campbell, and V. Piksaikin. 1998. *An eight-group delayed neutron model based on a consistent set of half-lives*. LA-UR-98-1619. Los Alamos, NM: Los Alamos National Laboratory.

Studsvik AB. n.d. SIMULATE-3K. *Studsvik.* https://www.studsvik.com/what-we-do/products/simulate3-k/.

Talley, D.G. 2017a. *RAZORBACK – A Research Reactor Transient Analysis Code v. 1.0 vol. 1: User's Manual*. SAND2017-10561. Albuquerque, NM: Sandia National Laboratories.

Talley, D.G. 2017b. *RAZORBACK – A Research Reactor Transient Analysis Code v. 1.0 vol. 3: Verification and Validation Report*. SAND2017-3372. Albuquerque, NM: Sandia National Laboratories.

Wagner, W., J.R. Cooper, A. Dittmann, J. Kijima, H.-J. Kretzschmar, A. Kruse, R. Mareš, K. Oguchi, H. Sato, I. Stöcker, O. Šifner, Y Takaishi, I. Tanishita, J. Trübenbach, Th. Willkommen. 2000. The IAPWS Industrial Formulation 1997 for the Thermodynamic Properties of Water and Steam. *Journal of Engineering for Gas Turbines and Power* 122 (1): 150–184. doi: 10.1115/1.483186.

Weast, R.C., and M.J. Astle. 1979. *CRC Handbook of Chemistry and Physics*. Boca Raton, FL: CRC Press.

Weck, P.F., E. Kim, V. Tikare, and J.A. Mitchell. 2015. Mechanical properties of zirconium alloys and zirconium hydrides predicted from density functional perturbation theory. *Dalton Transactions* 43:18769–18779. doi: 10.1039/C5DT03403E.

YMP (Yucca Mountain Project). 2003. *Disposal Criticality Analysis Methodology Topical Report.* YMP/TR-004Q, Rev. 2. Las Vegas, NV: Yucca Mountain Site Characterization Office.

This page is intentionally left blank